

1 **Influence of enhanced Asian NO<sub>x</sub> emissions on ozone in the Upper Troposphere and**  
2 **Lower Stratosphere (UTLS) in chemistry climate model simulations**

3 Chaitri R.<sup>1</sup>, Suvarna Fadnavis<sup>1\*</sup>, Rolf Müller<sup>2</sup>, Ayantika D. C.<sup>1</sup>, Felix Ploeger<sup>2</sup>, Alexandru Rap<sup>3</sup>

4 <sup>1</sup>Indian Institute of Tropical Meteorology, Pune, India

5 <sup>2</sup>Forschungszentrum Jülich GmbH, IEK7, Jülich, Germany

6 <sup>3</sup>School of Earth and Environment, University of Leeds, Leeds, United Kingdom

7 \*Email of corresponding author: suvarna@tropmet.res.in

8

9 **Abstract:**

10 **The Asian summer monsoon (ASM) anticyclone is the most pronounced circulation pattern in the**  
11 **Upper Troposphere and Lower Stratosphere (UTLS) during the Northern Hemisphere summer.** Asian  
12 summer monsoon convection plays an important role in efficient vertical transport from the surface to  
13 the upper-level anticyclone. In this paper we investigate the potential impact of enhanced  
14 anthropogenic nitrogen oxides (NO<sub>x</sub>) on the distribution of ozone in the UTLS using the fully-coupled  
15 aerosol chemistry climate model, ECHAM5-HAMMOZ. Ozone in the UTLS is influenced both by the  
16 convective uplift of ozone precursors and by the uplift of enhanced NO<sub>x</sub> induced tropospheric ozone  
17 anomalies. We performed anthropogenic NO<sub>x</sub> emission sensitivity experiments over India and China.  
18 **In these simulations, covering the years 2000-2010 anthropogenic NO<sub>x</sub> emissions have been increased**  
19 **by 38% over India and by 73% over China with respect to the emission base year 2000. These emission**  
20 **increases are comparable to the observed linear trends of 3.8 % per year over India and 7.3% per year**  
21 **over China during the period 2000 to 2010. Enhanced** NO<sub>x</sub> emissions over India by 38 % and China by  
22 73 % increase the ozone radiative forcing in the ASM Anticyclone (15°-40°N, 60°-120°E) by 16.3 mW  
23 m<sup>-2</sup> and 78.5 mW m<sup>-2</sup> respectively. These elevated NO<sub>x</sub> emissions **produce** significant warming over the  
24 Tibetan Plateau and increase precipitation over India due to a strengthening of the monsoon Hadley

25 circulation.

26 However increase in NO<sub>x</sub> emissions over India by 73% (similar to the observed increase over China),  
27 results in large amount of ozone production over the Indo Gangetic plain and Tibetan Plateau. The  
28 higher ozone concentrations, in turn, induce a reversed monsoon Hadley circulation and negative  
29 precipitation anomalies over India. The associated subsidence suppresses vertical transport of NO<sub>x</sub> and  
30 ozone into the ASM anticyclone.

31 Key words: Asian summer monsoon, Tropospheric ozone, Tropospheric NO<sub>x</sub>, NO<sub>x</sub> transport, Upper  
32 troposphere and lower stratosphere, Ozone radiative forcing.

33

## 34 1. Introduction

35 Rapid economic development and urbanization in Asia has resulted in an unprecedented growth in  
36 anthropogenic emissions of nitrogen oxides (NO<sub>x</sub>), carbon monoxide (CO), carbon dioxide (CO<sub>2</sub>),  
37 methane (CH<sub>4</sub>). Many of these species affect concentrations of tropospheric ozone, which is both an  
38 important polluting agent and a greenhouse gas (Wild and Akimoto, 2001; Chatani et al 2014; Revell et  
39 al., 2015). Ground based and satellite observations show a large amount of these ozone precursors  
40 concentrated over India and China (Sinha et al., 2014; Richter et al., 2005; Jacob et al., 1999; Zhao et  
41 al., 2013; Gu et al., 2014). Studies show that tropospheric ozone production over Asia is controlled by  
42 the abundance of NO<sub>x</sub> and VOCs (Sillman, 1995, Lei et al., 2004, Zhang et al., 2004 and Tie et al.,  
43 2007), with large regions such as India and China being NO<sub>x</sub> limited regions. Therefore, increased NO<sub>x</sub>  
44 in these regions leads to an increase in ozone concentrations (Yamaji et al., 2006; Sinha et al., 2014;  
45 Fadnavis et al., 2014). Recently, positive trends in Asian tropospheric column NO<sub>2</sub> have been reported,  
46 i.e. 3.8 % yr<sup>-1</sup> over India, using SCanning Imaging Absorption SpectroMeter for Atmospheric  
47 CHartography (SCIAMACHY) observations for the period 2003-2011 (Ghude et al., 2013), and 7.3%  
48 yr<sup>-1</sup> over China using Ozone Monitoring Instrument (OMI) observations for the period 2002-2011

49 (Schneider and van der A., 2012). Lightning contributes to the production of NO<sub>x</sub> in the middle and  
50 upper troposphere (Barret et al, 2016). Over the Asian region, lightning contributes ~40% to NO<sub>x</sub> and  
51 20% to ozone production in the middle and upper troposphere during the monsoon season (Tie et al.  
52 2001; Fadnavis et al. 2015). The upper tropospheric ozone concentration is determined by in-situ  
53 production from both lightning and ozone precursors which are transported from the boundary layer  
54 (Sóvde et al., 2011; Barret et al, 2016).

55 Tropospheric ozone has a warming effect on climate, its estimated radiative forcing due to  
56 increased concentrations since pre-industrial times being 0.4 W m<sup>-2</sup>, with a 5 to 95% confidence range  
57 of (0.2 to 0.6 W m<sup>-2</sup>) (Stevenson et al., 2013; Myhre et al., 2013). Previous studies highlighted the  
58 importance of the tropical tropopause region for ozone radiative forcing (Lacis et al, 1990; Riese et al.,  
59 2012; Rap et al., 2015) and showed that ozone perturbations exert a large influence on the thermal  
60 structure of the atmosphere (e.g., Thuburn and Craig, 2002; Foster and Shine 1997). A recent study  
61 based on Atmospheric Chemistry and Climate Model Intercomparison Project (ACCMIP) models  
62 reported that NO<sub>x</sub> and CH<sub>4</sub> are the greatest contributors in determining tropospheric ozone radiative  
63 forcing (Stevenson et al., 2013).

64 Asian Summer Monsoon (ASM) convection efficiently transports Asian pollutants from the  
65 boundary layer into the Upper Troposphere and Lower Stratosphere (UTLS) (Randel and Park, 2006;  
66 Randel et al. 2010; Fadnavis et al., 2013, 2015). Studies pertaining to modeling and trajectory analysis  
67 confirm this finding (Li et al., 2005; Park et al., 2007; Randel et al., 2010; Chen et al., 2012; Vogel et  
68 al., 2015, 2016). Satellite observations show the confinement of a number of chemical constituents like  
69 water vapor (H<sub>2</sub>O), CO, CH<sub>4</sub>, ethane, hydrogen cyanide (HCN), PAN and aerosols, within the ASM  
70 anticyclone (Park et al., 2004, 2007, 2008; Li et al., 2005; Randel and Park, 2006; Xiong et al., 2009;  
71 Randel et al. 2010; Lawrence et al., 2011; Abad et al., 2011; Fadnavis et al., 2013;2014;2015; Barret et  
72 al., 2016) which has potential implications on stratospheric chemistry and dynamics. Thus the rise in

73 anthropogenic emissions over the ASM region alters the chemical composition of the UTLS (Lawrence  
74 et al., 2011; Fadnavis et al., 2014, 2015) during the monsoon season. Another prominent feature of the  
75 satellite observations is an ozone minimum in the ASM anticyclone (near 100 hPa) (Gettelman et al.,  
76 2004; Konopka et al., 2010; Braesicke et al., 2011). This ozone minimum is linked to upward transport  
77 of ozone poor air masses (Gettelman et al., 2004; Park et al., 2007; Kunze et al., 2010). Observations  
78 show that convectively lifted air masses arriving in the anticyclone are ozone poor but rich in ozone  
79 precursors. Balloon sonde observations show that ozone variations near the anticyclone are strongly  
80 correlated with temperature near the tropopause (Tobo et al., 2008). Thus the linkage of low ozone and  
81 high concentrations of ozone precursors with the temperature variation in the anticyclone is an open  
82 question.

83 In this study we ask the question ‘how do increasing Asian NO<sub>x</sub> emissions and the associated  
84 ozone production affect ozone radiative forcing and monsoon circulation?’. We perform sensitivity  
85 experiments of increased anthropogenic NO<sub>x</sub> emissions using the state-of-the-art ECHAM5-HAMMOZ  
86 (European Centre General Circulation Model version5) chemistry climate model (Roeckner et al.,  
87 2003; Horowitz et al., 2003; Stier et al., 2005). We estimate the ozone radiative forcing for the different  
88 anthropogenic NO<sub>x</sub> emission scenarios, together with associated changes in temperature and the  
89 monsoon circulation. The paper is organized as follows: in Section 2 the data and model set up are  
90 described; the results are summarized in Section 3 and discussed in Section 4, followed by conclusions  
91 given in Section 5.

## 93 **2. Data description and Model setup**

### 94 **2.1 Satellite measurements**

95 Earth Observing System (EOS) microwave limb sounder (MLS) is one of the four instruments  
96 on the NASA’s EOS Aura satellite flying in the polar sun-synchronous orbit. It measures the thermal

97 emissions at millimeter and sub millimeter wavelengths (Waters et al., 2006). It performs 240 limb  
98 scans per orbit with a footprint of ~6 km across-track and ~200 km along-track, providing ~3500  
99 profiles per day. MLS also measures vertical profiles of temperature, ozone, CO, H<sub>2</sub>O, and many other  
100 constituents in the mesosphere, stratosphere and upper troposphere (Waters et al., 2006). In the UTLS,  
101 MLS has a vertical resolution of **about** 3 km. MLS vertical profiles of ozone show good agreements  
102 with the Stratospheric Aerosol and Gas Experiment II (SAGE-II), Halogen Occultation Experiment  
103 (HALOE), Atmospheric Chemistry Experiment (ACE) and ozonesonde measurements (Froidevaux et  
104 al.,2006). The MLS ozone profiles are considered to be useful in the range of 215 – 0.46 hPa (Livesey  
105 et al., 2005). In this study we analyze the MLS level 2 (version 4) ozone mixing ratios data for the  
106 period 2004 – 2013. **The data has been interpolated to potential temperature levels and gridded**  
107 **horizontally, within latitude bins of equal area (with the equatorial bin of 150km width) and longitude**  
108 **bins of about 8.5 degrees.** This data can be accessed from <http://mls.jpl.nasa.gov/>. For comparison,  
109 simulated ozone is convolved with the MLS averaging kernel (Livesey et al. 2011).

110

## 111 **2.2 Model simulation and experimental setup**

112 We employ the aerosol-chemistry-climate model ECHAM5-HAMMOZ which comprises the  
113 general circulation model ECHAM5 (Roeckner et al., 2003), the tropospheric chemistry module,  
114 **MOZART2** (Horowitz et al 2003) and the aerosol module, Hamburg aerosol model (HAM) (Stier et al.,  
115 2005). It includes NO<sub>x</sub>, VOC and aerosol chemistry. The gas phase chemistry is based on the chemical  
116 scheme provided by the MOZART-2 model (Horowitz et al., 2003) which includes detailed chemistry  
117 of the O<sub>x</sub>-NO<sub>x</sub> hydrocarbon system with 63 tracers and 168 reactions. The O(<sup>1</sup>D) quenching reaction  
118 rates used are taken from Sander et al., (2003) and isoprene nitrates chemistry taken from Fiore et al.,  
119 (2005). The dry deposition in ECHAM5-HAMMOZ follows the scheme given by Ganzeveld and  
120 Lelieveld (1995). Soluble trace gases like HNO<sub>3</sub> and SO<sub>2</sub> are also subject to wet deposition. In-cloud

121 and below-cloud scavenging follows the scheme given by Stier et al. (2005). **Interactive calculation of**  
122 **cloud droplet number concentration is according to Lohmann et al (1999) and ice crystal number**  
123 **concentrations are according to Kärcher and Lohmann (2002). The convection scheme is based on the**  
124 **mass flux scheme developed by Tiedke (1989).**

125  
126 The model is run at a T42 spectral resolution corresponding to about  $2.8^\circ \times 2.8^\circ$  in the horizontal  
127 dimension and 31 vertical hybrid  $\sigma - p$  levels from the surface to 10 hPa. **In our model simulations,**  
128 **emissions from anthropogenic sources and biomass burning are from the year 2000 RETRO project**  
129 **data set (available at <http://eccad.sedoo.fr/>) (Schultz et al., 2004; 2005; 2007; 2008). Emissions of SO<sub>2</sub>,**  
130 **BC and OC are based on the AEROCOM-II emission inventory, also for the year 2000 (Dentener et al.,**  
131 **2006). The distribution of NO<sub>x</sub> emission mass flux ( $\text{kg m}^{-2} \text{s}^{-1}$ ) averaged for the Asian summer**  
132 **monsoon season (June–September) is shown in Supplementary Fig. S1. It shows high values over the**  
133 **Indo Gangetic Plains and East China.** Other details of model parameterizations, emissions and  
134 **evaluation** are described by Fadnavis et al. (2013; 2014; 2015) and Pozzoli et al. (2008a, b; 2011). Each  
135 of our model experiments consists of continuous simulations for eleven years from 2000 to 2010. **The**  
136 **base year for emissions is taken as 2000 and emissions were repeated every year throughout the**  
137 **simulation period.** Meteorology varied due to **varying monthly** mean sea surface temperature (SST) and  
138 sea ice concentration (SIC). The AMIP2 SSTs and SIC **varying for** the period 2000 – 2010 were  
139 specified as a lower boundary condition.

140 In order to understand the impact of enhanced **anthropogenic** NO<sub>x</sub> emissions on the distribution  
141 of ozone in the UTLS, **sensitivity** simulations were performed for the period 2000 – 2010. The  
142 experimental set up is the same as described by Fadnavis et al., (2015). The four **simulations** analyzed  
143 in this study are: (1) a reference experiment (CTRL) and three sensitivity experiments (referred to as  
144 experiments 2 - 4), where the **anthropogenic** NO<sub>x</sub> emissions over India and China are scaled in  
145 accordance with the observed trends. In experiment (2), **anthropogenic** NO<sub>x</sub> emissions are increased

146 over India by 38% (Ind38), in experiment (3) increases-over China by 73% (Chin73) are prescribed. In  
147 order to analyze the effects of similar NO<sub>x</sub> percentage increases over India and China, NO<sub>x</sub> emissions  
148 are increased over India by 73% (Ind73) in experiment (4). The emission perturbations were obtained  
149 from observed NO<sub>2</sub> trends of 3.8% per year over India (Ghude et al., 2013) and 7.3% per year over  
150 China (Schneider and van der A., 2012). Hiboll et al. (2013) also reported similar increasing NO<sub>x</sub>  
151 values over megacities in India and China. All four simulations use the same VOC and CO emissions  
152 and they all include NO<sub>x</sub> production due to lightning (lightning-on) and soil emissions (see Table 1,  
153 showing details pertaining to these experiments). Therefore NO<sub>x</sub> or ozone anomalies obtained from  
154 difference between Ind38, Ind73 and Chin73 with respective to CTRL simulation do not have an  
155 impact of lightning or soil emissions as they are same in all the simulations.

156 In addition, a series of four lightning-off simulations were performed for the same period and  
157 boundary conditions as experiments 1-4 (these simulations are the same as the ones documented by  
158 Fadnavis et al. (2015))The impact of lightning on NO<sub>x</sub> production is estimated by comparing the CTRL  
159 (lightning-on) simulation with lightning-off simulations.

160 The accuracy of the simulation of the monsoon circulation will likely depend on the model  
161 resolution and increased vertical resolution may improve the model performance (Druyan et al., 2008;  
162 Abhik et al., 2014). While we acknowledge the limitations of our relatively course vertical resolution  
163 (dictated by our computational resources), the model is still capable of reasonably simulating the  
164 general regional spatial pattern of precipitation and low-level circulation (Rajeevan et al., 2005) (see  
165 Supplementary Fig. S2, showing simulated seasonal mean precipitation and circulation at 850 hPa in  
166 the CTRL simulation).

167 The heating rates and radiative forcings associated with the ozone changes in our three  
168 sensitivity simulations are calculated using the Edwards and Slingo (1996) radiative transfer model and  
169 the fixed dynamical heating approximation for stratospheric temperature adjustment. Similarly to

170 previous studies (Riese et al., 2012; Bekki et al., 2013; Rap et al., 2015), we used the off-line version of  
171 the model, with six shortwave and nine longwave bands, and a delta-Eddington 2-stream scattering  
172 solver at all wavelengths.

173

## 174 **3. Results**

### 175 **3.1 Comparison with MLS satellite measurements in the UTLS**

176 The spatial distributions of ozone mixing ratios from MLS observations at 100 hPa and from  
177 the CTRL ECHAM5-HAMMOZ simulation at 90 hPa (the nearest model level) after smoothing with  
178 the averaging kernel of MLS are illustrated in Fig. 1a and Fig. 1b, respectively. The climatological  
179 horizontal winds plotted in the figure clearly show the anticyclonic upper level monsoon circulation.  
180 Recent attempts to characterize the extent of the anticyclone are based either on potential vorticity on  
181 isentropic surfaces or geopotential height on pressure surfaces. Here we apply both characterizations of  
182 the anticyclone and show the PV contour related to the maximum PV gradient on 380K (calculated  
183 from ERA-Interim reanalysis following Ploeger et al., 2015), and the 270m geopotential height  
184 anomaly as proposed by Barret et al. (2016). The close agreement of both methods shows that from a  
185 climatological point of view the two criteria yield a very similar picture of the anticyclonic circulation  
186 and the related trace gas confinement. Locally and at particular dates, however, differences may be  
187 larger with potential vorticity correlating better with confined trace gas anomalies than geopotential  
188 height (e.g., Garny and Randel, 2013; Ploeger et al., 2015). The spatial pattern of low ozone  
189 concentrations in the monsoon anticyclone is well simulated in the model. It is in good agreement with  
190 MLS (90-140 ppbv), MIPAS (80-120 ppbv) and SAGE II (<150ppbv) measurements (Kunze et al.,  
191 2010; Randel et al., 2001; Randel and Park 2006; Park et al., 2007).

192 Vertical profiles of ozonesonde measurements (averaged for the monsoon season during 2001-  
193 2009) at Indian stations, Delhi (28.61°N, 77.23°E), Pune (18.52°N, 73.85°E) and Thiruvananthapuram



194 (8.48°N, 76.95E) are compared with MLS measurements and ECHAM5-HAMMOZ simulated ozone  
195 mixing ratios in Figs. 1(c)-(e). ECHAM5-HAMMOZ simulations show good agreement with MLS data  
196 between 200 hPa and 50 hPa at all three stations. Comparison of ozonesonde observations with the  
197 ECHAM5-HAMMOZ simulation shows reasonably good agreement at Pune, compared to Delhi and  
198 Thiruvananthapuram where there are some discrepancies. The simulated ozone mixing ratios are lower  
199 than ozonesonde measurements by 10-40 ppb between 500 – 90 hPa at Pune and by ~70-90 ppb in the  
200 upper troposphere (500-150 hPa) at Delhi. At Thiruvananthapuram, while at altitudes below 375 hPa,  
201 simulated ozone mixing ratios show good agreement with ozonesonde data, at the altitudes above 375  
202 hPa, simulated values are lower than observations by ~20-70 ppb. The differences between model and  
203 ozonesonde data may be due to different grid sizes: the ECHAM5-HAMMOZ model grid size is ~280  
204 km, while balloon observations are within ~30-180 km spatial range (balloon typically drifts ~30–180  
205 km horizontally). In addition, previous work comparing these model simulations with various aircraft  
206 observations during the monsoon season, found a reasonable agreement for PAN, NO<sub>x</sub>, HNO<sub>3</sub> and O<sub>3</sub>  
207 mixing ratios (Fadnavis et al., 2015).

208

### 209 **3.2 Transport of enhanced NO<sub>x</sub> emissions into the UTLS**

210 Recent satellite observations and model simulations quantified the impact of convective  
211 transport of boundary layer pollution into the ASM anticyclone during the Asian summer monsoon  
212 season (Gettelman et al., 2004; Randel et al., 2010; Fadnavis et al., 2013, 2014, 2015). These pollutants  
213 are further transported across the tropopause as evident in satellite observations of, e.g. water vapour  
214 (Bian, 2012), hydrogen cyanide (HCN) (Randel, 2010), CO (Schoeberl et al., 2006), Peroxyacetyl  
215 nitrate (PAN) (Fadnavis et al., 2014; 2015), aerosols (Vernier et al., 2015, Fadnavis et al., 2013). To  
216 understand the influence of monsoon convection on the vertical distribution of NO<sub>x</sub> we show zonal and  
217 meridional cross sections over India and China. Vertical distributions of NO<sub>x</sub> averaged for the monsoon

218 season over Indian latitudes (8°N-35°N), and Chinese latitudes (20°N-45°N) as obtained from CTRL  
219 simulations are shown in the Supplementary Figs. S3(a) and S3(b) respectively. These figures show  
220 elevated levels of NO<sub>x</sub> extending from the surface to the upper troposphere over India and China. The  
221 wind vectors along with the distribution of cloud droplet number concentration (CDNC) and ice crystal  
222 number concentration (ICNC), (Supplementary Figs. S4(a), S4(b) and S4(c)) indicate strong convective  
223 transport from the Bay of Bengal (BOB), South China Sea and southern slopes of Himalayas which  
224 might lift the boundary layer NO<sub>x</sub> to the upper troposphere.

225 During the monsoon season, the NO<sub>x</sub> distribution in the UTLS is also influenced by lightning,  
226 in addition to transport from anthropogenic sources. Lightning activity during this season was found to  
227 be more pronounced in Asia, compared to the other monsoon regions such as North America, South  
228 America and Africa (Ranalkar and Chaudhari, 2009; Penki and Kamra, 2013). In our simulations, we  
229 find that lightning produces 40-70% of NO<sub>x</sub> over north India and Bay of Bengal and 40-60% over the  
230 Tibetan Plateau and West China region (Supplementary Fig. S5).

231 Fig. 2 shows the vertical distribution of anthropogenic NO<sub>x</sub> anomalies obtained from the Ind38,  
232 Ind73, Chin73 simulations, compared with the CTRL simulation. Ind38 and Chin73 simulations show  
233 that the convective winds over the Bay of Bengal (80-90°E) (Figs. 2(a) and 2(c)) and at the southern  
234 flank\_of the Himalayas (Figs. 2(d) and 2(f)) lift up the enhanced NO<sub>x</sub> emissions to the upper  
235 troposphere (UT). While most transport is mainly into the UT, parts of it also occur into the lower  
236 stratosphere, with cross tropopause transport being particularly evident in the Chin73 simulation (Figs.  
237 2(c) and 2(f)). Randel and Park (2006) and Randel et al. (2010) also reported that pollution transported  
238 by Asian monsoon convection enters the stratosphere. Our results are also in good agreement with  
239 previous studies indicating significant vertical transport due to strong monsoon convection from the  
240 southern slopes of Himalayas (Fu et al., 2006, Fadnavis et al., 2013; 2014) and the South China Sea  
241 (Park et al 2009; Chen et al., 2012). In the upper troposphere, NO<sub>x</sub> is transported over Iran and Saudi

242 Arabia along the descending branch of the **large scale monsoon** circulation (Rodwell and Hoskins,  
243 1995). However, the cross tropopause transport is not present in the Ind73 simulation, where it is  
244 inhibited by the wind anomalies that show a descending branch over central India ( $\sim 20^\circ\text{N}$ ,  $75^\circ\text{E}$ ) (Figs.  
245 2(b) and 2(e)). These descending wind anomalies may also be related to the associated ozone radiative  
246 forcing and temperature changes, as discussed in Section 4.

247

### 248 **3.3 Impact of enhanced anthropogenic $\text{NO}_x$ on the tropospheric ozone distribution**

249 We **calculate** the change in ozone production over India and China due to enhanced  $\text{NO}_x$   
250 emissions in the Ind38, Ind73 and Chin73 simulations with respect to the CTRL **simulation**. Figure 3,  
251 showing longitude-pressure cross sections of net ozone production (ppt/day) changes, indicates that the  
252 majority of this additional ozone production occurs in the lower troposphere. At altitudes below 300  
253 hPa, the ozone production and loss vary between  $-15 \text{ ppt day}^{-1}$  and  $15 \text{ ppt day}^{-1}$ . In the upper  
254 troposphere (300-150 hPa), the estimated amount of **additional** net ozone production in Ind38 and  
255 Ind73 simulation is  $3\text{-}7 \text{ ppt day}^{-1}$ , while in the Chin73 simulation it is  $\sim 3\text{-}13 \text{ ppt day}^{-1}$ . We also simulate  
256 ozone loss near the tropopause in the Ind73 simulation (Figure 3b). We note that these ozone anomalies  
257 are not driven by lightning  $\text{NO}_x$ , as this is included in all simulations. **It is interesting to understand**  
258 **ozone production over the highly populated Indo Gangetic Plain and Tibetan Plateau region. A**  
259 **longitude pressure cross section over this region show that ozone production over the Indo Gangetic**  
260 **Plain and Tibetan Plateau in Ind73 is (20-25ppt/day) is much larger than Ind38 (6-20 ppt/day) in the**  
261 **lower troposphere (supplementary Fig. S6).**

262 **Figure 4** shows the vertical distribution of ozone anomalies induced by enhanced anthropogenic  
263  $\text{NO}_x$  emissions in the three perturbation experiments compared to the CTRL simulation, averaged over  
264 India and China. Although the air mass in the monsoon anticyclone is relatively poor in ozone  
265 (**Fig.1(b)**), the elevated amounts of ozone anomalies in response to enhanced anthropogenic  $\text{NO}_x$

266 emissions are clearly seen in Fig. 4. This may be partially due to convective transport of enhanced-  
267 NO<sub>x</sub>-emission induced ozone anomalies produced in the lower troposphere, and partially due to  
268 chemical ozone production from convectively transported boundary layer ozone precursors. Ozone  
269 anomalies are enhanced near 300-200 hPa over west Asia (40-60°E) (Figs. 4a-c), possibly due to the  
270 vertical convective transport of ozone anomalies and precursors and also from subsequent horizontal  
271 transport in the monsoon anticyclone (Barret et al., 2016).

272 Latitude-pressure cross sections of enhanced-NO<sub>x</sub>-emission induced ozone anomalies plotted in  
273 Figs. 4(d) and 4(f) illustrate how convection over the Bay of Bengal, the southern slopes of the  
274 Himalayas and the South China Sea lifts the enhanced ozone anomalies from India and China into the  
275 upper troposphere. These ozone anomalies are also transported further across the tropopause and into  
276 the lower stratosphere, where ozone production is also driven by photolysis and NO<sub>x</sub> anomalies.

277 In the Ind73 simulation, similarly to the NO<sub>x</sub> anomaly distribution (Figs. 2(b) and 2(e)), the  
278 descending branch of circulation over central India also suppresses the vertical transport of ozone  
279 anomalies across the tropopause (Figs. 4(b) and 4(e)). This subsidence may be related to ozone heating  
280 rate changes, as there is significant increase in ozone production over the Indo Gangetic plain and  
281 Tibetan Plateau in the lower troposphere due to enhanced anthropogenic NO<sub>x</sub> emissions (Section 4).

282

### 283 **3.4 Distribution of NO<sub>x</sub> and ozone in the anticyclone**

284 The distributions of NO<sub>x</sub> and ozone anomalies in the monsoon anticyclone region in the Ind38,  
285 Ind73 and Chin73 simulations with respect to the CTRL simulation are shown in Figs. 5(a)-(f). A  
286 maximum in the NO<sub>x</sub> anomalies in the ASM anticyclone (60°E to 120°E) is seen in all the simulations.  
287 NO<sub>x</sub> anomalies are high at the eastern part of the monsoon anticyclone since convective injection into  
288 the anticyclone occurs mainly in that region (Fadnavis et al., 2013). Increase in NO<sub>x</sub> anomalies in the  
289 Ind38 simulation is higher (Fig. 5(a)) than that in the Ind73 simulation (Figs. 5(b)), mainly due to

290 descending motion over central India in the Ind73 simulation, as seen in the previous sections. In  
291 contrast to NO<sub>x</sub> anomalies, ozone anomalies in Ind38 are lower than Ind73, especially in the north-  
292 eastern part of anticyclone. Satellite observations also show high ozone precursors and low ozone  
293 amounts in the anticyclone (Park et al., 2007; Barret et al., 2016). Similarly, the Chin73 simulation  
294 shows higher values of NO<sub>x</sub> anomalies (>18%) and strong negative ozone anomalies (~-8%) in the  
295 north eastern region of the monsoon anticyclone (Figs. 5(c) and 5(f)). Figure 5 also shows that the  
296 tropical easterly jet transports NO<sub>x</sub> and ozone (from India and China) to Saudi Arabia, Iran and Iraq.

297

#### 298 4. Discussion

299 To estimate the radiative impact of the simulated ozone changes, we use the offline version of  
300 the Edwards and Slingo (1996) radiative transfer model. Figure 6 shows the radiative forcing caused by  
301 the ozone changes in each of the three sensitivity simulations compared to the CTRL simulation. The  
302 overall increase in tropospheric ozone (see Figure 4) has a warming effect on climate, with the regional  
303 average radiative forcing in the monsoon anticyclone (15°N-40°N, 60-120°E) estimated at 16.3 mW m<sup>-2</sup>,  
304 69.9 mW m<sup>-2</sup>, and 78.5 mW m<sup>-2</sup> in the Ind38, Ind73, and Chin73 simulations, respectively.

305 We also investigate the impact on the atmospheric heating rates caused by the ozone changes.  
306 Figure 7 shows the zonal mean heating rate anomalies for the Ind38, Ind73 and Chin73 simulations,  
307 compared to the CTRL simulation. These three simulations show positive and negative heating rates  
308 anomalies between 400-200 hPa. However, in the upper troposphere and lower stratosphere (200-50  
309 hPa) ozone heating rates are negative over Indo Gangetic plain (20-30°N) and Tibetan Plateau (30-  
310 40°N) region. In Ind73 simulation, ozone heating rate anomalies are positive in the lower troposphere  
311 over the Indo Gangetic plain (1000-750 hPa) and Tibetan plateau (600-400 hPa). This may be due to  
312 large amount of ozone production in the lower troposphere over these regions (Fig. S6). This heating  
313 may produce changes in the circulation leading to ascending motion over the Tibetan Plateau and a

314 descending branch over central India ( $\sim 20^\circ\text{N}$ ), i.e. a reversal of monsoon Hadley circulation (Fig. 9(b)).

315 Figures 8 shows latitude pressure cross-section of temperature anomalies (K) obtained from  
316 Ind38, Ind73 and Chin73 simulations. Ind38 and Chin73 simulations show anomalous warming in the  
317 upper troposphere over the Tibetan Plateau while it is subdued in the Ind73 simulation. Upper  
318 tropospheric warming over the Tibetan plateau is one of the key factors responsible for the ASM  
319 circulation (Flohn 1957; Yanai et al., 1992; Meehl, 1994; Li and Yanai, 1996; Wu and Zhang, 1998).  
320 Flohn (1957, 1960) suggested that upper tropospheric warming over the Tibetan plateau leads to  
321 increased Indian summer monsoon rainfall by enhancing the cross-equatorial circulation that brings  
322 rainfall to India (Rajagopalan and Molnar, 2013, Vinoj et al., 2014). Goswami et al., (1999) also  
323 reported that there is a strong correlation between Hadley circulation and monsoon precipitation.

324 Figures 9(a)-(c) depict the change in monsoon Hadley cell circulation (averaged over  $70^\circ\text{E}$ -  
325  $100^\circ\text{E}$ ) obtained from the difference in the Ind38, Ind73 and Chin73 and CTRL simulations. The Ind38  
326 and Chin 73 simulations show a strengthening of the Hadley circulation; a strong ascending branch of  
327 the Hadley cell around  $10^\circ$ - $20^\circ\text{N}$  (Fig. 9(a)), whereas the tilted descending branch of Hadley cell is seen  
328 over  $20^\circ\text{N}$  in the Ind73 simulation (Fig. 9(b)). In Ind73 simulation ozone heating rates are positive and  
329 negative in the vertical direction near  $\sim 20^\circ\text{N}$  (Fig 7 (b)) which might have attributed tilted descending  
330 branch of Hadley cell. Consequently, precipitation anomalies over the Indian region ( $70^\circ$ - $90^\circ\text{E}$ ;  $8^\circ$ - $35^\circ$   
331  $\text{N}$ ) are positive ( $0.3$  to  $0.9\text{ mm day}^{-1}$ ) in the Ind38 and Chin73 simulations (Figs. 9(d) and 9(f)), whereas  
332 they are negative in the Ind73 simulation ( $-0.3$  to  $-0.6\text{ mm day}^{-1}$ ) (Fig. 9(e)). In the upper troposphere  
333 ( $250\text{ hPa}$ - $100\text{ hPa}$ ), Ind73 simulation shows subsidence while Chin73 simulation shows ascending  
334 motion at these levels over the Indian region. Upper tropospheric subsidence in Ind73 simulation might  
335 have contributed to the weak positive and negative precipitation anomalies over the North Indian  
336 region (Fig. 9(e)). The Chin73 simulation shows subsidence near  $22^\circ\text{N}$  below  $200\text{ hPa}$  and ascending  
337 motion above it. The Chin73 simulation shows ascending motion near  $12^\circ\text{N}$  rising up to  $110\text{ hPa}$ , which

338 leads to positive precipitation anomalies over the Indian peninsula.

339 Thus, enhanced Indian (Ind38) and Chinese (Chin73) NO<sub>x</sub> emissions increase warming over the  
340 Tibetan plateau and enhance precipitation over India via a strengthening of the monsoon Hadley  
341 circulation. Remarkably, a further increase of NO<sub>x</sub> emissions over India (Ind73) leads to high amounts  
342 of ozone in the lower troposphere over the Indo Gangetic plain and Tibetan Plateau. The related ozone  
343 heating induces a reversal of the monsoon Hadley circulation, thereby resulting in negative  
344 precipitation anomalies.

## 345 5. Conclusions

346 In this paper we investigate the potential impacts of enhanced anthropogenic NO<sub>x</sub> emissions on  
347 ozone production and distribution during the monsoon season using the state-of-the-art ECHAM5-  
348 HAMMOZ model simulations. We performed sensitivity experiments for anthropogenic NO<sub>x</sub>  
349 enhancements of 38% over India (Ind38 simulation) and 73% over China (Chin73 simulation) in  
350 accordance with recently observed trends of 3.8% per year over India and 7.3% per year over China  
351 (Ghude et al., 2013; Schneider and van der A., 2012). In another experiment, anthropogenic NO<sub>x</sub>  
352 emissions over India are increased by 73%, equal to Chinese emissions (Ind73 simulation).

353 These simulations show that an increase in anthropogenic NO<sub>x</sub> emissions (over India and  
354 China) increases ozone production in the lower and mid-troposphere. The monsoon convection at the  
355 southern flank of the Himalayas (80-90°E) and over the Bay of Bengal lifts up the NO<sub>x</sub> and ozone  
356 anomalies from India across the tropopause into the lower stratosphere. Cross tropopause transport also  
357 occurs over China due to convection over the South China Sea.

358 Increase in NO<sub>x</sub> emissions in the Ind38, Ind73 and Chin73 simulations leads to increase in  
359 ozone radiative forcings, in the anticyclone (15°N-40°N, 60°E-120°E) of 16.25 mWm<sup>-2</sup>, 69.88 mW m<sup>-2</sup>,  
360 and 78.51 mW m<sup>-2</sup> in the Ind38, Ind73, and Chin73 simulations, respectively. Enhanced ozone

361 production (Ind38 and Chin73 simulations) increases ozone heating rates which cause anomalous  
362 warming over the **Tibetan plateau**. Further increase in NO<sub>x</sub> emissions over the India region (Ind73  
363 simulation) produces anomalous heating in the lower troposphere over the Indo Gangetic Plain and  
364 Tibetan Plateau. **This warming elicits the reversal of the monsoon Hadley cell circulation. The**  
365 **descending branch of the monsoon Hadley circulation over the central India impedes vertical transport**  
366 **of ozone and NO<sub>x</sub> anomalies.**

367 In the Ind38 and Chin73 simulations, anomalous warming over the **Tibetan plateau** results in a  
368 strengthening of the monsoon Hadley circulation over India and elicits positive precipitation (0.3 to 0.9  
369 mm day<sup>-1</sup>) anomalies over India. However, in Ind73 simulations the reversal of the Hadley circulation  
370 and the concurrent subdued warming in the upper troposphere over the **Tibetan plateau** results in  
371 negative precipitation anomalies (-0.3 to -0.6 mm day<sup>-1</sup>) over India.

372

373 *Acknowledgement:* Dr. S. Fadnavis and C. Roy acknowledges with gratitude Dr. Krishnan, Director of  
374 IITM, for his encouragement during the course of this study. We also thank **two** anonymous reviewers  
375 for their valuable suggestions for improvement of this manuscript. Authors acknowledge the High  
376 Power Computing Centre (HPC) in IITM, Pune, India, for providing computer resources. **Part of the**  
377 **research leading to these results has received funding from the European Community's Seventh**  
378 **Framework Programme (FP7/2007-2013) in the frame of the StratoClim project under grant agreement**  
379 **number 603557. Felix Ploeger was supported by the Helmholtz Young Investigators Group grant A-**  
380 **SPECi (VH-NG-1128).**

381



382 **References:**

- 383 Abad G. G., Allen N. D. C., Bernath P. F., Boone C. D., McLeod S. D., Manney G. L., Toon G. C.,  
384 Carouge C., Wang Y., Wu S., Barkley M. P., Palmer P. I., Xiao Y., and Fu T. M.: Ethane, ethyne  
385 and carbon monoxide concentrations in the upper troposphere and lower stratosphere from ACE  
386 and GEOS-Chem: a comparison study, *Atmos. Chem. Phys.*, 11, 9927–9941, 2011.  
387 doi:10.5194/acp-11-9927-2011, 2011.
- 388 Abhik S., Mukhopadhyay P., Goswami B. N., Evaluation of mean and intraseasonal variability of  
389 Indian summer monsoon simulation in ECHAM5: identification of possible source of bias,  
390 *Climate Dynamics*, Volume 43, Issue 1, pp 389–406, 2014.
- 391 Barret, B., Sauvage, B., Bennouna, Y., and Le Flochmoen, E.: Upper-tropospheric CO and O<sub>3</sub> budget  
392 during the Asian summer monsoon, *Atmos. Chem. Phys.*, 16, 9129-9147, doi:10.5194/acp-16-  
393 9129-2016, 2016.
- 394 Bekki, S., Rap, A., Poulain, V., Dhomse, S., Marchand, M., Lefevre, F., Forster, P. M., Szopa, S. and  
395 Chipperfield, M. P.: Climate impact of stratospheric ozone recovery, *Geophys. Res. Lett.*,  
396 40(11),2796-2800,doi:10.1002/grl.50358,2013.
- 397 Bian, J., Pan, L. L., Paulik, L., Vömel, H., Chen, H., and Lu, D.: In situ water vapor and ozone  
398 measurements in Lhasa and Kunming during the Asian summer monsoon, *Geophys. Res.*  
399 *Lett.*, 39, L19808, doi:10.1029/2012GL052996, 2012.
- 400 Braesicke, P., Smith, O. J., Telford, P., & Pyle, J. A.: Ozone concentration changes in the Asian  
401 summer monsoon anticyclone and lower stratospheric water vapour: An idealised model study.  
402 *Geophysical Research Letters*, 38(3), doi: 10.1029/2010GL046228, 2011.
- 403 Chatani, S., Amann, M., Goel, A., Hao, J., Klimont, Z., Kumar, A., Mishra, A., Sharma, S., Wang, S.  
404 X., Wang, Y. X., and Zhao, B.: Photochemical roles of rapid economic growth and potential  
405 abatement strategies on tropospheric ozone over South and East Asia in 2030, *Atmos. Chem.*  
406 *Phys.*, 14, 9259-9277, doi:10.5194/acp-14-9259-2014, 2014.
- 407 Chen, B., Xu, X., D, Yang, S., and Zhao, T. L.: Climatological perspectives of air transport from  
408 atmospheric boundary layer to tropopause layer over Asian monsoon regions during boreal  
409 summer inferred from Lagrangian approach, *Atmos. Chem. Phys.*, 12, 5827–5839,  
410 doi:10.5194/acp-12-5827-2012. 2012.
- 411 Dentener F., Kinne S., Bond T., Boucher O., Cofala J., Generoso S., Ginoux P., Gong S., Hoelzemann  
412 J. J., Ito A., Marelli L., Penner J. E., Putaud J.-P., Textor C., Schulz M., Werf G. R. van der, and  
413 Wilson J.: Emissions of primary aerosol and precursor gases in the years 2000 and 1750  
414 prescribed data-sets for AeroCom, *Atmos. Chem. Phys.*, 6, 4321-4344, doi:10.5194/acp-6-  
415 4321-2006, 2006.
- 416 Druyan L. M., Fulakeza M. and Lonergan P.: The impact of vertical resolution on regional model  
417 simulation of the west African summer monsoon, *Int. J. Climatol.* 28: 1293–1314, DOI:  
418 10.1002/joc.1636, 2008.
- 419 Edwards, J. M., and Slingo, A.: Studies with a flexible new radiation code .1. Choosing a  
420 configuration for a large-scale model, *Quart. Jour. Roy. Met. Soc.*, 122(531), 689-719,  
421 doi:10.1002/qj.49712253107,1996.
- 422 Fadnavis, S., Semeniuk, K., Pozzoli, L., Schultz, M. G., Ghude, S. D., Das, S., and Kakatkar, R.:  
423 Transport of aerosols into the UTLS and their impact on the Asian monsoon region as seen in a  
424 global model simulation, *Atmos. Chem. Phys.*, 13, 8771–8786, doi:10.5194/acp-13-8771-2013,  
425 2013.
- 426 Fadnavis, S., Semeniuk, K., Schultz, M. G., Kiefer, M., Mahajan, A., Pozzoli, L., and Sonbawane, S.:  
427 Transport pathways of peroxyacetyl nitrate in the upper troposphere and lower stratosphere  
428 from different monsoon systems during the summer monsoon season. *Atmos. Chem. and*

429 Phys., 15, doi:10.5194/acp-15-11477-2015, 11477-11499, 2015.

430 Fadnavis, S., Semeniuk, K., Schultz, M. G., Mahajan, A., Pozzoli, L., Sonbawane, S., and Kiefer, M.:  
 431 Transport pathways of peroxyacetyl nitrate in the upper troposphere and lower stratosphere  
 432 from different monsoon systems during the summer monsoon season, *Atmos. Chem. Phys.*  
 433 *Discuss.*, 14, 20159–20195, doi:10.5194/acpd-14-20159-2014, 2014.

434 Fiore, A. M., Horowitz, L. W., Purves, D. W., Levy II, H., Evans, M. J., Wang, Y., Li, Q., and  
 435 Yantosca, R. M.: Evaluating the contribution of changes in isoprene emissions to surface ozone  
 436 trends over the eastern United States, *J. Geophys. Res.*, 110, D12303,  
 437 doi:10.1029/2004JD005485, 2005.

438 Flohn, H.: Large-scale aspects of the summer monsoon in South and East Asia, *J. Meteor. Soc. Japan*,  
 439 75, 180–186, doi: 551.553.21:551.589.5, 1957.

440 Flohn, H.: Recent investigations on the mechanism of the “Summer Monsoon” of Southern and  
 441 Eastern Asia, *Proc. Symp. Monsoon of the World*, 1960.

442 Forster, F., Piers, M., and Keith, P. Shine: Radiative forcing and temperature trends from stratospheric  
 443 ozone changes, *J. Geophys Res*, 102, 10841-10855, 1997.

444 Froidevaux, L., Livesey, N. J., Read, W. G., Jiang, Y. B., Jimenez, C. J., Filipiak, M. J., Schwartz, M.  
 445 J., Santee, M. L., Pumphrey, H. C., Jiang, J. H., Wu, D. L., Manney, G. L., Drouin, B. J.,  
 446 Waters, J. W., Fetzer, E. J., Bernath, P. F., Boone, C. D., Walker, K. A., Jucks, K. W., Toon, G.  
 447 C., Margitan, J. J., Sen, B., Webster, C. R., Christensen, L. E., Elkins, J. W., Atlas, E., Ueb, R.  
 448 A., and Hendershot, R.: Early validation analyses of atmospheric profiles from EOS MLS on  
 449 the Aura satellite. *IEEE Trans. Geosci. Remote Sensing* 44, 1106 – 1121, doi:  
 450 10.1109/TGRS.2006.864366, 2006.

451 Fu, R., Hu, Y. L., Wright, J. S., Jiang, J. H., Dickinson, R.E., Chen, M. X., Filipiak, M., Read, W. G.,  
 452 Waters, J. W., and Wu, D. L.: Short circuit of water vapor and polluted air to the global  
 453 stratosphere by convective transport over the Tibetan Plateau, *P. Natl. Acad. Sci. USA*, 103,  
 454 5664–5669, doi:10.1073/pnas.0601584103, 2006.

455 Ganzeveld, L. and Lelieveld, J.: Dry deposition parameterization in a chemistry general circulation  
 456 model and its influence on the distribution of reactive trace gases, *J. Geophys. Res.*, 100,  
 457 20999–21012, doi:10.1029/95JD02266, 1995.

458 Garny, H. and Randel, W. J.: Dynamic variability of the Asian monsoon anticyclone observed in  
 459 potential vorticity and correlations with tracer distributions, *J. Geophys. Res. Atmos.*, 118,  
 460 13,421–13,433, doi:10.1002/2013JD020908, 2013.

463 Gettelman, A., Kinnison, D. E., Dunkerton, T. J., and Brasseur, G. P.: Impact of monsoon circulations  
 464 on the upper troposphere and lower stratosphere, *J. Geophys. Res.*, 109, D22101,  
 465 doi:10.1029/2004jd004878, 2004.

466 Ghude, S. D., Kulkarni, S. H., Jena, C., Pfister, G. G., Beig, G., Fadnavis, S., and van der A R. J.:  
 467 Application of satellite observations for identifying regions of dominant sources of nitrogen  
 468 oxides over the Indian Subcontinent, *J. Geophys. Res.*, 118, 1–15, doi:10.1029/2012JD017811,  
 469 2013.

470 Goswami, B. N., Krishnamurthy, V., and Annamalai, H.: A broad-scale circulation index for the  
 471 interannual variability of the Indian summer monsoon. *Q. J. R. Meteorol. soc.*, 125, 611-633,  
 472 doi: 10.1002/qj.49712555412, 1999.

473 Gu, D., Wang, Y., Smeltzer, C., and Boersma, K. F.: Anthropogenic emissions of NO<sub>x</sub> over China:  
 474 Reconciling the difference of inverse modeling results using GOME-2 and OMI  
 475 measurements, *J. Geophys. Res. Atmos.*, 119, doi:10.1002/ 2014JD021644, 2014.

478 Hilboll, A., Richter, A., and Burrows, J. P.: Long-term changes of tropospheric NO<sub>2</sub> over megacities  
 479 derived from multiple satellite instruments, *Atmos. Chem. Phys.*, 13, 4145–4169,  
 480 doi:10.5194/acp-13-4145-2013, 2013.

481 Horowitz, L. W., Walters, S., Mauzerall, D. L., Emmons, L. K., Rasch, P. J., Granier, C., Tie, X.,  
482 Lamarque, J., Schultz, M. G., Tyndall, G. S., Orlando, J. J., and Brasseur, G. P.: A global  
483 simulation of tropospheric ozone and related tracers, Description and evaluation of MOZART,  
484 version 2, *J. Geophys. Res.*, 108, 4784, doi:10.1029/2002JD002853, 2003.

485 Jacob, D. J., Logan, J. A., and Murti, P. P.: Effect of rising Asian emissions on surface ozone in the  
486 United States, *Geophys. Res. Lett.*, 26, 2175–2178, doi:10.1029/1999GL900450, 1999.

487 **Kärcher B. and U. Lohmann, A parameterization of cirrus cloud formation: Homogeneous freezing of**  
488 **supercooled aerosols, *J. Geophys. Res.* 107, NO. D2, 4010, 10.1029/2001JD000470, 2002.**

489 Konopka, P., Groß, J.U., Günther, G., Ploeger, F., Pommrich, R., Müller, R. and Livesey, N.: Annual  
490 cycle of ozone at and above the tropical tropopause: observations versus simulations with the  
491 Chemical Lagrangian Model of the Stratosphere (CLaMS), *Atmos. Chem. Phys.*, 10(1), 121-  
492 132, doi: www.atmos-chem-phys.net/10/121/2010/, 2010.

493 Kunze, M., Braesicke, P., Langematz, U., Stiller, G., Bekki, S., Brühl, C., Chipperfield, M., Dameris,  
494 M., Garcia, R. and Giorgetta, M.: Influences of the Indian summer monsoon on water vapor  
495 and ozone concentrations in the UTLS as simulated by chemistry-climate models, *J. Clim.*,  
496 23(13), 3525-3544, doi: http://dx.doi.org/10.1175/2010JCLI3280.1, 2010.

498 Lacis Andrew, A., Donald Wuebbles, J., and Jennifer Logan A., Radiative Forcing of climate by  
499 Changes in the Vertical Distribution of Ozone, *J. Geophys. Res.*, 95 , 9971-9981, doi:  
500 10.1029/JD095iD07p09971, 1990.

501 Lawrence, M. G.: Atmospheric science: Asia under a high-level brown cloud, *Nat. Geosci.*, 4, 352–  
502 353, doi:10.1038/ngeo1166, 2011.

503 Lei, W., Zhang, R., Tie, X., and Hess, P.: Chemical characterization of ozone formation in the  
504 Houston-Galveston area. *J. Geophys. Res.*, 109, doi: 10.1029/2003JD004219, 2004.

505 Li, C. and Yanai M.: The onset and interannual variability of the Asian summer monsoon in relation to  
506 land–sea thermal contrast, *J. Clim.* 9: 358–375, doi: http://dx.doi.org/10.1175/1520-  
507 0442(1996)009<0358:TOAIVO>2.0.CO;2, 1996.

508 Li, Q., Jiang, J. H., Wu, D. L., Read, W. G., Livesey, N. J., Waters, J. W., Zhang, Y., Wang, B.,  
509 Filipiak, M. J., Davis, C. P., Turquety, S., Wu, S., Park, R. J., Yantosca, R. M., and Jacob, D. J.:  
510 Convective outflow of south Asian pollution: a global CTM simulation compared with EOS  
511 MLS observations, *Geophys. Res. Lett.*, 32, doi: http://dx.doi.org/10.1029/2005GL022762,  
512 doi: 10.1029/2005GL022762, 2005.

513 Livesey, N. J., Read, W. G., Filipiak, M. J., Froidevaux, L., Harwood, R. S., Jiang, J. H., Jimenez, C.,  
514 Pickett, H. M., Pumphrey, H. C., Santee, M. L., Schwartz, M. J., Waters, J. W., and Wu, D. L.:  
515 EOS MLS Version 1.5 Level 2 data quality and description document, JPL, California, 2005.

516 **Livesey, N. J., Read, W. G., Froidevaux, L., Lambert, A., Manney, G. L., Pumphrey, H. C., Santee, M.**  
517 **L., Schwartz, M. J., Wang, S., Cofield, R. E., Cuddy, D. T., Fuller, R. A., Jarnot, R. F., Jiang, J.**  
518 **H., Knosp, B. W., Stek, P. C., Wagner, P. A., and Wu, D. L.: Version 3.3 Level 2 data quality**  
519 **and description document. Tech Rep. JPL D-33509, Jet Propulsion Laboratory, available at:**  
520 **http://mls.jpl.nasa.gov (last access: 17 August 2015), 2011.**

521 **Lohmann, U., J. Feichter, C. C. Chuang, and J. E. Penner, Predicting the number of cloud droplets in**  
522 **the ECHAM GCM, *J. Geophys. Res.*, 104, 9169 – 9198, 1999.**

523 Meehl, G. A.: Coupled land-ocean-atmosphere processes and South Asian monsoon variability,  
524 *Science*, 266, 263–267, doi: 10.1126/science.266.5183.263, 1994.

525 **Myhre, G., et al., Anthropogenic and natural radiative forcing, in *Climate Change 2013: The Physical***  
526 **Science Basis. Contribution of Working Group I to the Fifth Assessment Report of the**  
527 **Intergovernmental Panel on Climate Change, edited by T. F. Stocker et al., pp. 659–740,**  
528 **Cambridge Univ. Press, Cambridge, U. K., and New York, 2013.**

533 **Park, M., Randel, W. J., Emmons, L. K., Bernath, P. F., Walker, K. A., and Boone, C. D.: Chemical**

534 isolation in the Asian monsoon anticyclone observed in Atmospheric Chemistry Experiment  
535 (ACE-FTS) data, *Atmos. Chem. Phys.*, 8, 3, 757-764, doi: [www.atmos-chem-](http://www.atmos-chem-phys.net/8/757/2008/)  
536 [phys.net/8/757/2008/](http://www.atmos-chem-phys.net/8/757/2008/), 2008.

537 Park, M., Randel, W. J., Emmons, L. K., and Livesey, N. J.: Transport pathways of carbon monoxide in  
538 the Asian summer monsoon diagnosed from Model of Ozone and Related Tracers (MOZART),  
539 *J. Geophys. Res.*, 114, D08303, doi:10.1029/2008jd010621, 2009.

540 Park, M., Randel, W. J., Gettelman, A., Massie, S. T., and Jiang, J.H.: Transport above the Asian  
541 summer monsoon anticyclone inferred from Aura Microwave Limb Sounder tracers, *J.*  
542 *Geophys. Res.*, 112, D16309, doi:10.1029/2006jd008294, 2007.

543 Park, M., Randel, W. J., Kinnison, D. E., Garcia, R. R., and Choi, W.: Seasonal variation of methane, water vapour, and  
544 nitrogen oxides near the tropopause: Satellite observations and model simulations, *J. Geophys. Res.*, 109,  
545 D03302, doi:10.1029/2003JD003706, 2004.

546 Penki, R. K. and Kamra, A. K.: Lightning distribution with respect to the monsoon trough position  
547 during the Indian summer monsoon season, *J. Geophys. Res.*, 118, 4780–4787,  
548 doi:10.1002/jgrd.50382, 2013.

549 Ploeger, F., Gottschling, C., Griessbach, S., Groß, J.-U., Guenther, G., Konopka, P., Müller, R., Riese,  
550 M., Stroh, F., Tao, M., Ungermann, J., Vogel, B., and von Hobe, M.: A potential vorticity-based  
551 determination of the transport barrier in the Asian summer monsoon anticyclone, *Atmos.*  
552 *Chem. Phys.*, 15, 13145-13159, doi:10.5194/acp-15-13145-2015, 2015.

553 Pozzoli, L., Bey, I., Rast, J. S., Schultz, M. G., Stier, P., and Feichter, J.: Trace gas and aerosol  
554 interactions in the fully coupled model of aerosol-chemistry-climate ECHAM5- HAMMOZ: 1.  
555 Model description and insights from the spring 2001 TRACE-P experiment, *J. Geophys. Res.*,  
556 113, D07308, doi:10.1029/2007JD009007, 2008a.

557 Pozzoli, L., Bey, I., Rast, J. S., Schultz, M. G., Stier, P., and Feichter, J.: Trace gas and aerosol  
558 interactions in the fully coupled model of aerosol-chemistry-climate ECHAM5- HAMMOZ: 2.  
559 Impact of heterogeneous chemistry on the global aerosol distributions, *J. Geophys. Res.*, 113,  
560 D07309, doi:10.1029/2007JD009008, 2008b.

561 Pozzoli, L., Janssens-Maenhout, G., Diehl, T., Bey, I., Schultz, M. G., Feichter, J., Vignati, E., and  
562 Dentener, F.: Re-analysis of tropospheric sulfate aerosol and ozone for the period 1980–2005  
563 using the aerosol-chemistry-climate model ECHAM5-HAMMOZ, *Atmos. Chem. Phys.*, 11,  
564 9563–9594, doi:10.5194/acp-11-9563-2011, 2011.

565 Rajeevan M., Bhatte J., Kale J.D and Lal B.: Development of High Resolution Daily Gridded Rainfall  
566 Data for the Indian Region, *Met. Monograph Climatology No. 22/2005*, National Climate  
567 Centre India Meteorological Department. Pune 411 005, India, 2005.

568 Rajagopalan, B., and Molnar, P.: Signatures of Tibetan Plateau heating on Indian summer monsoon  
569 rainfall variability, *J. Geophys. Res. Atmos.*, 118, 1170–1178, doi:10.1002/jgrd.50124, 2013.

570 Ranalkar, M. R. and Chaudhari, H. S.: Seasonal variation of lightning activity over the Indian  
571 subcontinent, *Meteorol. Atmos. Phys.*, 104, 125–134, doi: 10.1007/s00703-009-0026-7, 2009.

572 Randel, W. J., and Park M.: Deep convective influence on the Asian summer monsoon anticyclone and  
573 associated tracer variability observed with Atmospheric Infrared Sounder (AIRS), *J. Geophys.*  
574 *Res.*, 111, D12314, doi:10.1029/2005JD006490, 2006.

575 Randel, W. J., Park, M., Emmons, L., Kinnison, D., Bernath, P., Kaley Walker, A., Boone, C., and  
576 Pumphrey, H.: Asian Monsoon Transport of Pollution to the Stratosphere *Science*, 328(5978),  
577 611-613, doi: 10.1126/science.1182274, 2010.

578 Randel, W. J., Wu, F., Gettelman, A., Russell, J. M., Jawodny, J. M., and Oltmans, S. J.: Seasonal  
579 variation of water vapor in the lower stratosphere observed in Halogen Occultation Experiment  
580 data, *J. Geophys. Res.*, 106, 14,313 – 14,325, doi: 10.1029/2001JD000485, 2001.

581 Rap, A., Richards, N., A., D., Forster, P., M., Monks, S., Arnold, S., R., Chipperfield, M.: Satellite

582 constraint on the tropospheric ozone radiative effect, *Geophys. Res. Lett.*, 42, [5074-5081](https://doi.org/10.1002/2015GL064037).doi:10.1002/2015GL064037, 2015.

583

584 Revell, L. E., Tummon, F., Stenke, A., Sukhodolov, T., Coulon, A., Rozanov, E., Garny, H., Grewe, V.,  
585 and Peter, T.: Drivers of the tropospheric ozone budget throughout the 21st century under the  
586 medium-high climate scenario RCP 6.0, *Atmos. Chem. Phys.*, 15, 5887-5902, doi:10.5194/acp-  
587 15-5887-2015, 2015.

588 Richter, A., John Burrows, P., Hendrik, N., Granier C., and Niemeier, U.: Increase in tropospheric  
589 nitrogen dioxide over China observed from space; 437, doi:10.1038/nature04092, 2005.

590 Riese, M., Ploeger, F., Rap, A., Vogel, B., Konopka, P., Dameris, M. and Forster, P.: Impact of  
591 uncertainties in atmospheric mixing on simulated UTLS composition and related radiative  
592 effects, *J. Geophys. Res.: Atmos.*, 117(D16), doi: 10.1029/2012JD017751, 2012.

593 Rodwell, M. J. and Hoskins, B. J.: Monsoons and the dynamics of deserts, *QJRMS*, 122(534), 1385-  
594 1404, doi: 10.1002/qj.49712253408, 1995.

595 Roeckner, E., Bauml, G., Bonaventura, L., Brokopf, R., Esch, M., Giorgetta, M., Hagemann, S.,  
596 Kirchner, I., Kornbluh, L., Manzini, E., Rhodin, A., Schlese, U., Schulzweida, U., and  
597 Tompkins, A.: The atmospheric general circulation model ECHAM5: Part 1, Tech. Rep. 349,  
598 Max Planck Institute for Meteorology, Hamburg, 2003.

599 Sander, S. P., Fried, R. R., Barker, J. R., Golden, D. M., Kurylo, M. J., Wine, P. H., J. Abbatt, P. D., 25  
600 Burkholder, J. B., Kolb, C. E., Moortgat, G. K., Huie, R. E., and Orkin, V. L.: Chemical  
601 kinetics and photochemical data for use in atmospheric studies, evaluation number 14, JPL  
602 Publ. 02-25, Jet Propul. Lab., Calif. Inst. Of Technol., Pasadena, available at:  
603 [http://jpldataeval.jpl.nasa.gov/pdf/JPL\\_02-25\\_rev02.pdf](http://jpldataeval.jpl.nasa.gov/pdf/JPL_02-25_rev02.pdf), 2003.

604 Schneider, P. and van der A. R. J.: A global single-sensor analysis of 2002–2011 tropospheric nitrogen  
605 dioxide trends observed from space, *J. Geophys. Res.*, 117, D16309,  
606 doi:10.1029/2012JD017571, 2012.

607 Schoeberl, M. R., Duncan, B. N., Douglass, A. R., Waters, J., Livesey, N., Read, W., and Filipiak, M.:  
608 The carbon monoxide tape recorder. *Geophys. Res. Lett.*, 33(12), doi:  
609 10.1029/2006GL026178, 2006.

610 Schultz, M. G., Heil, A., Hoelzemann, J. J., Spessa, A., Thonicke, K., Goldammer, J. G., Held, A. C.,  
611 Pereira, J. M. C., and van het Bolscher, M.: Global wildland fire emissions from 1960 to 2000,  
612 *Global Biogeochem. Cy.*, 22, GB2002, doi:10.1029/2007GB003031, 2008.

613 Schultz, M., Backman, L., Balkanski, Y., Bjoerndalsaeter, S., Brand, R., Burrows, J., Dalsoeren, S., de  
614 Vasconcelos, M., Grodtmann, B., Hauglustaine, D., Heil, A., Hoelzemann, J., Isaksen, I.,  
615 Kaurola, J., Knorr, W., Ladstaetter-Weienmayer, A., Mota, B., Oom, D., Pacyna, J., Panasiuk,  
616 D., Pereira, J., Pulles, T., Pyle, J., Rast, S., Richter, A., Savage, N., Schnadt, C., Schulz, M.,  
617 Spessa, A., Staehelin, J., Sundet, J., Szopa, S., Thonicke, K., van het Bolscher, M., van Noije,  
618 T., van Velthoven, P., Vik, A. and Wittrock, F.: REanalysis of the TROospheric chemical  
619 composition over the past 40 years (RETRO). A long-term global modeling study of  
620 tropospheric chemistry. Final Report, Tech. rep., Max Planck Institute for Meteorology,  
621 Hamburg, Germany, 2007.

622 Schultz, M.G., Heil A., Hoelzemann, J. J., Spessa, A., Thonicke, K., Goldammer, J., Held, A.C,  
623 Pereira, J. M., Van Het Bolscher, M.: Global Wildland Fire Emissions from 1960 to 2000,  
624 doi:10.1029/2007GB003031 , *Global Biogeochemical Cycles* 22 (GB2002) : 17 PP, 2005

625 Sillman, S.: The use of NO<sub>y</sub>, H<sub>2</sub>O<sub>2</sub>, and HNO<sub>3</sub> as indicators for ozone-NO<sub>x</sub>-hydrocarbon sensitivity in  
626 urban locations. *J. Geophys. Res.*, 100, 14,175–14,188, doi: 10.1029/94JD02953, 1995.

627 Sinha, V., Kumar, V., and Sarkar, C.: Chemical composition of pre-monsoon air in the Indo-Gangetic  
628 Plain measured using a new air quality facility and PTR-MS: high surface ozone and strong  
629 influence of biomass burning, *Atmos. Chem. Phys.*, 14, 5921–5941, 2014. doi:10.5194/acp-14-

630 5921-2014, 2014.

631 Søvde, O. A., Hoyle, C. R., Myhre, G., and Isaksen, I. S. A.: The HNO<sub>3</sub> forming branch of the HO<sub>2</sub> +  
632 NO reaction: pre-industrial-to-present trends in atmospheric species and radiative forcings,  
633 *Atmos. Chem. Phys.*, 11, 8929–8943, 2011; doi:10.5194/acp-11-8929-2011, 2011.

634 Stevenson, D. S., P. J. Young, Vaishali, N., Lamarque, J. F., Drew, T., Shindell, Voulgarakis, A., and  
635 Skeie R. B.: Tropospheric ozone changes, radiative forcing and attribution to emissions in the  
636 Atmospheric Chemistry and Climate Model Intercomparison Project (ACCMIP), *Atmos.*  
637 *Chem. Phys.*, 13, 3063-3085, doi:10.5194/acp-13-3063-2013, 2013.

638 Stier, P., Feichter, J., Kinne, S., Kloster, S., Vignati, E., Wilson, J., Ganzeveld, L., Tegen, I., Werner,  
639 M., Balkanski, Y., Schulz, M., Boucher, O., Minikin, A., and Petzold, A.: The aerosol-climate  
640 model ECHAM5-HAM, *Atmos. Chem. Phys.*, 5, 1125–1156, doi:10.5194/acp-5-1125-2005,  
641 2005.

642 Thuburn, J. and Craig, G.C.: On the temperature structure of the tropical stratosphere, *Journal of*  
643 *Geophysical Research: Atmospheres*, 107(D2), doi: 10.1029/2001JD000448, 2002.

644 Tie, X. X., Zhang, R., Brasseur, G., Emmons, L., and Lei, W.: Effects of lightning on reactive nitrogen  
645 and nitrogen reservoir species in the troposphere, *J. Geophys. Res.-Atmos.*, 106, 3167– 3178,  
646 doi:10.1029/2000JD900565, 2001.

647 Tie, X., Madronich, S., Li, G.H., Ying, Z.M., Zhang, R., Garcia, A., Lee-Taylor, and J., Y. Liu.  
648 Characterizations of chemical oxidants in Mexico City: a regional chemical/dynamical model  
649 (WRF-Chem) study, *Atmos. Environ.*, 41, 1989–2008, doi:10.1016/j.atmosenv.2006.10.053,  
650 2007.

651 **Tiedtke, M.: A comprehensive mass flux scheme for cumulus parameterization in large-scale models,**  
652 ***Mon. Weather Rev.*, 117(8), 1779–1800, 1989.**

653 Tobo, Y., Iwasaka, Y., Zhang, D., Shi, G., Kim, Y. S., Tamura, K., and Ohashi, T.: Summertime  
654 “ozone valley” over the Tibetan Plateau derived from ozonesondes and EP/TOMS data,  
655 *Geophys. Res. Lett.*, 35, L16801, doi:10.1029/2008GL03434, 2008.

656 Vernier, J.-P., T. D. Fairlie, M. Natarajan, F. G. Wienhold, J. Bian, B. G. Martinsson, S. Crumeyrolle,  
657 L. W. Thomason, and Bedka, K.: Increase in upper tropospheric and lower stratospheric  
658 aerosol levels and its potential connection with Asian Pollution, *J. Geophys. Res. Atmos.*, 120,  
659 1608–1619, doi:10.1002/2014JD022372, 2015.

660 Vinoj, V., Rasch, P.J., Wang, H., Yoon, J.H., Ma, P.L., Landu, K. and Singh, B.: Short-term modulation  
661 of Indian summer monsoon rainfall by West Asian dust, *Nature Geoscience*, 7(4), 308-313,  
662 doi:10.1038/ngeo2107, 2014.

663 Vogel B., Günther G., Müller R., Groöß, and Riese M.: Impact of different Asian source regions on the  
664 composition of the Asian J.-u. monsoon anticyclone and of the extratropical lowermost  
665 stratosphere, *Atmos. Chem. Phys.*, 15, 13699–13716, doi:10.5194/acp-15-13699-2015, 2015.

666 **Vogel, B., Günther, G., Müller, R., Groöß, J.-U., Afchine, A., Bozem, H., Hoor, P., Krämer, M., Müller,**  
667 **S., Riese, M., Rolf, C., Spelten, N., Stiller, G. P., Ungermann, J., and Zahn, A.: Long-range**  
668 **transport pathways of tropospheric source gases originating in Asia into the northern lower**  
669 **stratosphere during the Asian monsoon season 2012, *Atmos. Chem. Phys. Discuss.*,**  
670 **doi:10.5194/acp-2016-463, revised paper accepted for ACPD, 2016.**

671 Waters, J. W., Froidevaux, L., Harwood, R.S., Jarnot, R.F., Pickett, H. M., Read, W. G., Siegel, P. H.,  
672 Cofield, R. E., Filipiak, M. J., Flower, D. A., Holden, J. R., Lau, G. K., Livesey, N. J., Manney,  
673 G. L., Pumphrey, H. C., Santee, M. L., Wu, D. L., Cuddy, D. T., Lay, R. R., Loo, M. S., Perun,  
674 V. S., Schwartz, M. J., Stek, P. C., Thurstans, R. P., Boyles, M. A., Chandra, S., Chavez, M. C.,  
675 Chen, G. S., Chudasama, B. V., Dodge, R., Fuller, R. A., Girard, M.A., Jiang, J. H., Jiang, Y.,  
676 Knosp, B. W., LaBelle, R. C., Lee, K. A., Miller, D., Oswald, J. E., Patel, N. C., Pukala, D.  
677 M., Quintero, O., Scaff, D. M., Snyder, W. V., Tope, M. C., Wagner, P. A., and Walch, M. J.:

679 The Earth Observing System Microwave LimbSounder (EOS MLS) on the Aura satellite.  
680 IEEE Trans, Geosci., Remote Sensing, 44, 1075 – 1092, doi: 10.1109/TGRS.2006.873771,  
681 2006.

682 Wild, O., and Akimoto, H.: Intercontinental transport of ozone and its precursors in a three-  
683 dimensional global CTM, *J. Geophys. Res.*, 106(D21), 27729-27744, doi:  
684 <http://dx.doi.org/10.1029/2000JD000123>, 2001.

685 Wu, G. X., and Zhang, Y. S.: Tibetan Plateau forcing and the timing of the monsoon onset over South  
686 Asia and the South China Sea, *Mon Wea Rev* 126:913–927, doi:  
687 [http://dx.doi.org/10.1175/1520-0493\(1998\)126<0913:TPFATT>2.0.CO;2](http://dx.doi.org/10.1175/1520-0493(1998)126<0913:TPFATT>2.0.CO;2), 1998.

688 Xiong, X., Houweling S., Wei J., Maddy E., Sun F., and Barnet C.: Methane plume over south Asia  
689 during the monsoon season: satellite observation and model simulation, *Atmos. Chem. Phys.*,  
690 9, 783–794, doi:10.5194/acp-9-783-2009, 2009.

691 Yamaji, K., T. Ohara, I. Uno, H. Tanimoto, J. Kurokawa, and Akimoto H.: Analysis of the seasonal  
692 variation of ozone in the boundary layer in East Asia using the Community Multiscale Air  
693 Quality model: what controls surface ozone levels over Japan?, *Atmos. Environ.*, 40, 1856–  
694 1868, 2006.

695 Yanai, M., Li, C., Song, Z.: Seasonal heating of the Tibetan Plateau and its effects on the evolution of  
696 the Asian summer monsoon, *J Meteor Soc Japan*, 70, 189–221, 1992.

697 Zhang, R.W., Lei, X., and Hess, T. P.: Industrial emissions cause extreme diurnal urban ozone  
698 variability. *Proc. Natl. Acad. Sci.*, 101, 6346–6350, doi: 10.1073/pnas.0401484101, 2004.

699 Zhao, B., Wang, S. X., Liu, H., Xu, J. Y., Fu, K., Klimont, Z., Hao, J. M., He, K. B., Cofala, J., and  
700 Amann, M.: NO<sub>x</sub> emissions in China: historical trends and future perspectives, *Atmos. Chem.*  
701 *Phys.*, 13, 9869–9897, doi:10.5194/acp-13-9869-2013, 2013.

702

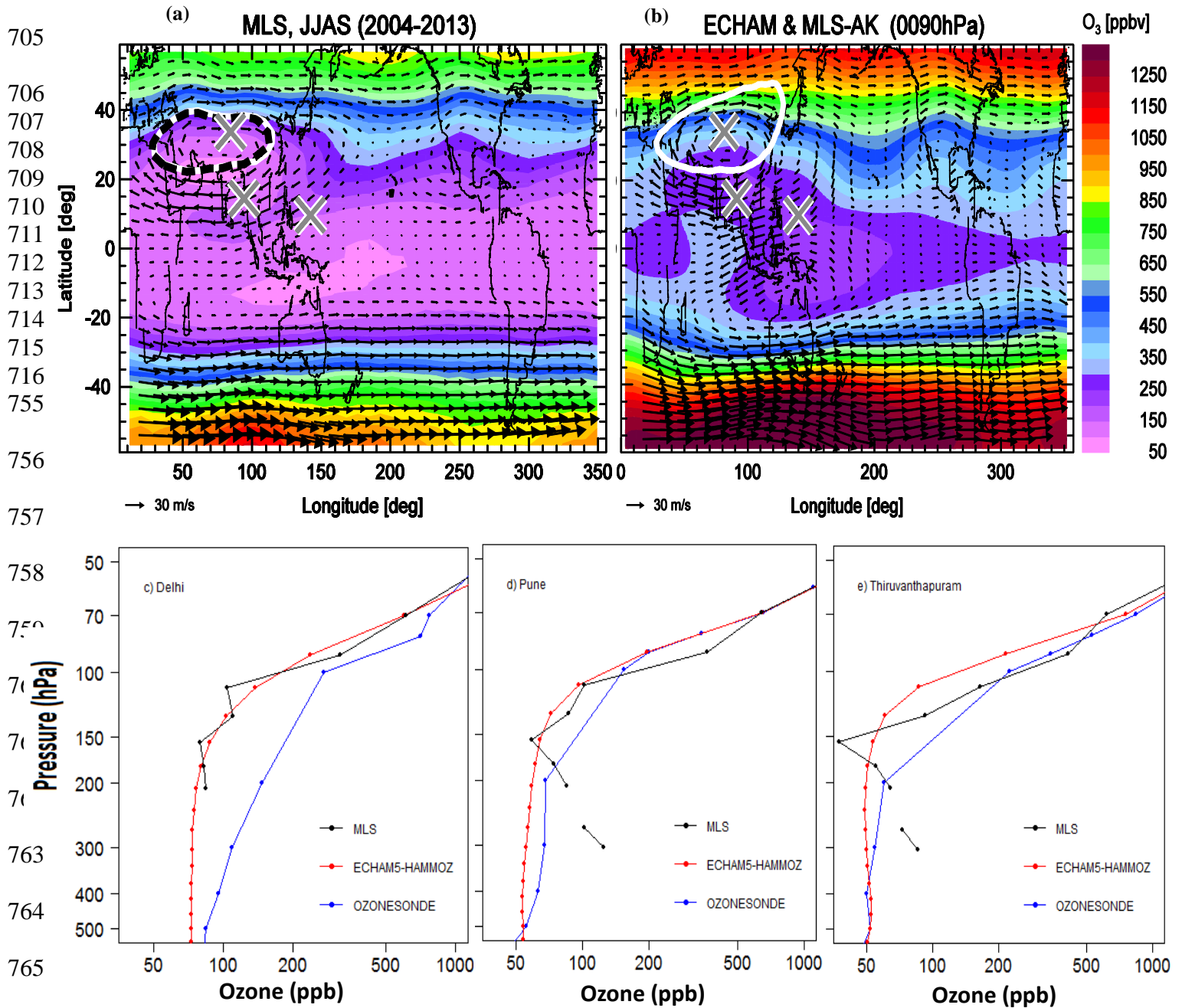
703

Table 1: Details of the sensitivity experiments (2000 - 2010).

<b>Name of experiment</b>	<b>Prescribed SSTs</b>	<b>Emissions</b>
CTRL	AMIP2 SST and SIC varying from 2000 – 2010	RETRO anthropogenic NO <sub>x</sub> emissions for the year 2000.
Ind38	AMIP2 SST and SIC varying from 2000 – 2010	RETRO anthropogenic NO <sub>x</sub> emissions for the year 2000 are increased by 38% over India for 11 years period 2000-2010
Chin73	AMIP2 SST and SIC varying from 2000 – 2010	RETRO anthropogenic NO <sub>x</sub> emissions for the year 2000 are increased by 73% over China for 10 years period 2000-2010.
Ind73	AMIP2 SST and SIC varying from 2000 – 2010	RETRO anthropogenic NO <sub>x</sub> emissions for the year 2000 are increased by 73% over India for 10 years period 2000-2010.

704





767 Figure 1: Distribution of ozone mixing ratio (ppb) during the monsoon season (June-September)  
 768 obtained from (a) MLS observations at 100 hPa, and (b) from ECHAM-HAMMOZ at 90hPa. Black  
 769 arrows indicate wind vectors, the black dashed contour shows the PV-gradient based transport barrier  
 770 of the anticyclone (calculated following Ploeger et al., 2015), and the white contour shows the 270m  
 771 geopotential height anomaly, corresponding to the anticyclone edge definition by Barret et al. (2016)  
 772 (Meteorological data shows climatological July fields from ERA-Interim reanalysis (a) ERA-Interim

773 reanalysis and (b) ECHAM5-HAMMOZ. The ECHAM5-HAMMOZ ozone distribution is smoothed  
774 using the MLS averaging kernel. Grey crosses highlight the regions of the Tibetan plateau, Bay of  
775 Bengal and South China Sea. Bottom panels show the vertical distribution of seasonal (June-  
776 September) mean ozone mixing ratios (ppb) from ozonesonde (2001-2009), MLS (2004-2013) and  
777 ECHAM5-HAMMOZ CTRL simulation at the (c) Delhi, (d) Pune, and (e) Thiruvananthpuram Indian  
778 stations.  
779

780

781

782

783

784

785

786

787

788

789

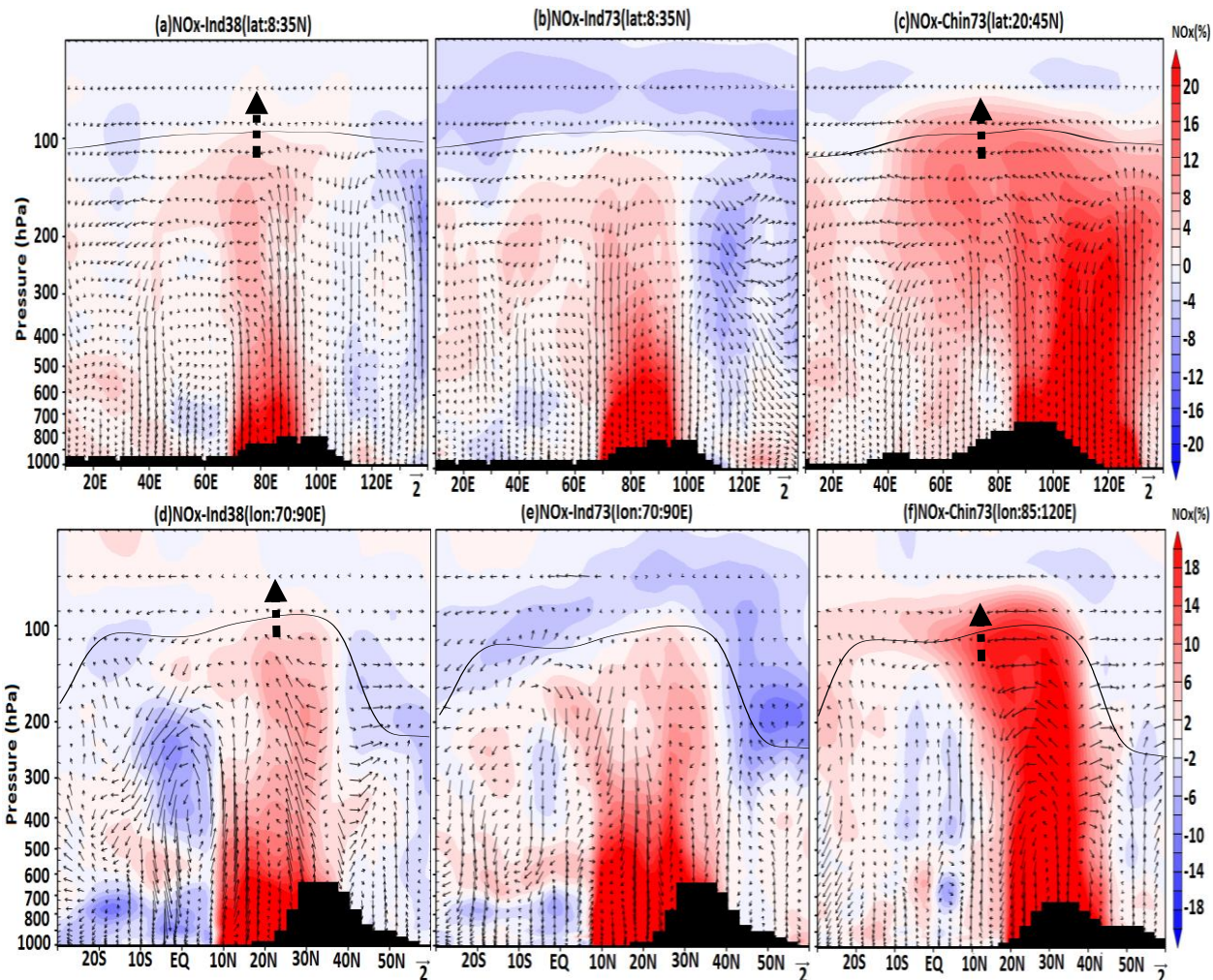
790

791

792

793

794



795 Figure 2: Longitude pressure cross-sections of percentage  $\text{NO}_x$  anomalies averaged for the monsoon

796 season (June-September) obtained from (a) Ind38 (averaged over  $8^\circ\text{N}$ - $35^\circ\text{N}$ ), (b) Ind73 (averaged over

797  $8^\circ\text{N}$ - $35^\circ\text{N}$ ), and (c) Chin73 (averaged over  $20^\circ\text{N}$ - $45^\circ\text{N}$ ) simulations. Latitude pressure cross-sections of

798 percentage  $\text{NO}_x$  anomalies averaged for the monsoon season (June-September) obtained from (d)

799 Ind38 (averaged over  $70^\circ\text{E}$ - $90^\circ\text{E}$ ), (e) Ind73 (averaged over  $70^\circ\text{E}$ - $90^\circ\text{E}$ ), and (f) Chin73 (averaged over

800  $85^\circ\text{E}$ - $120^\circ\text{E}$ ) simulations. Black arrows indicate wind vectors (the vertical velocity field has been

801 scaled by 300), the black line represents the tropopause, and the black dashed arrows indicate the cross

802 tropopause transport.

803

804

805

806

807

808

809

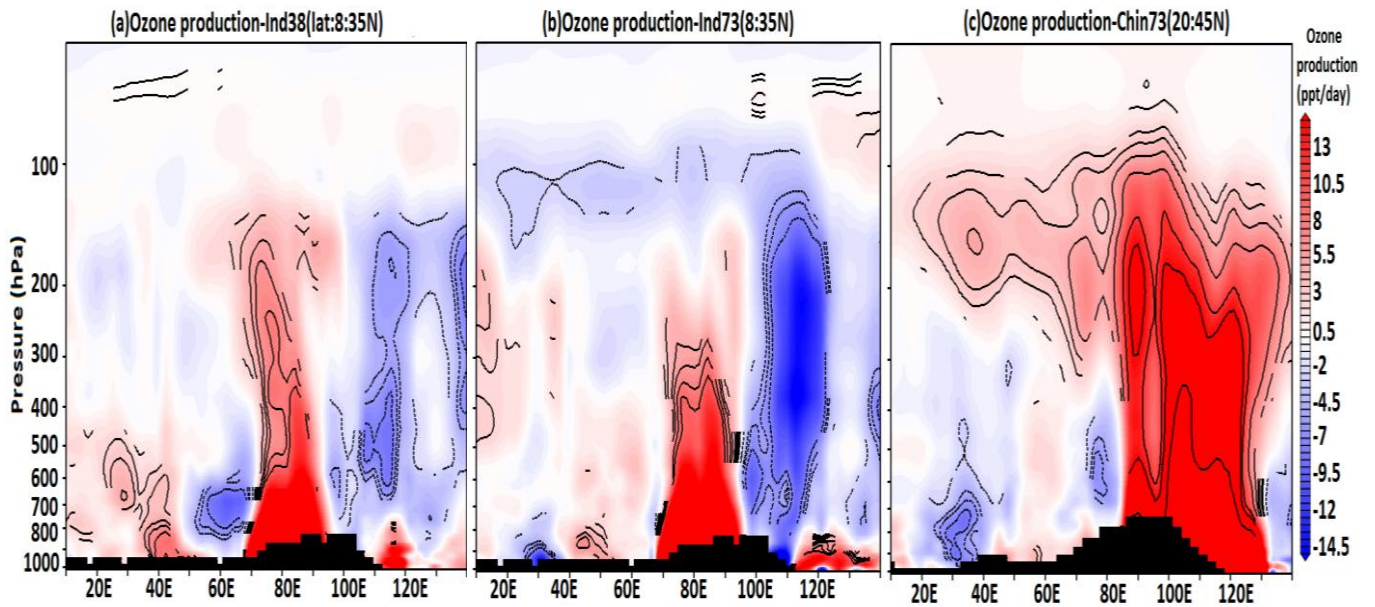
810

811

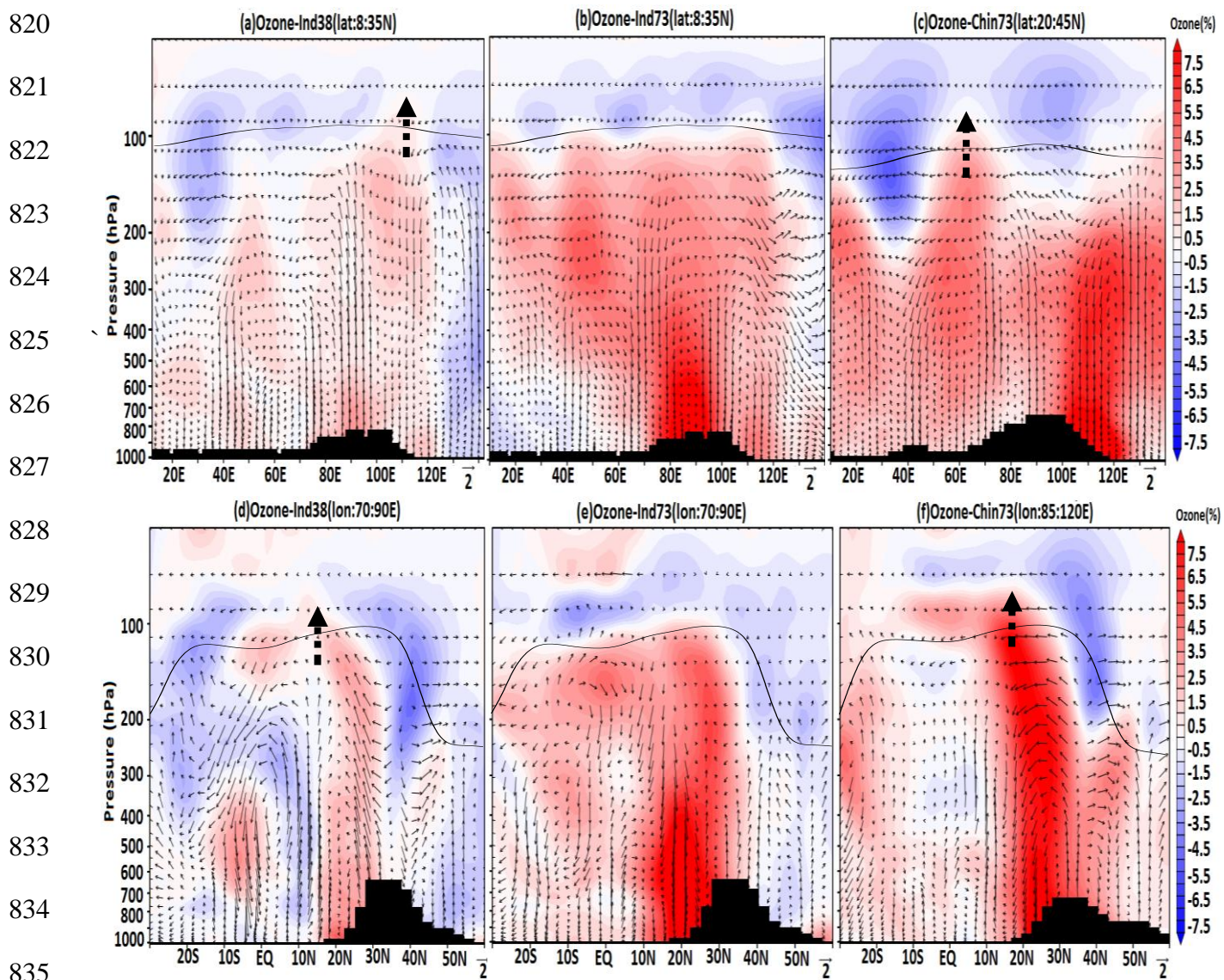
812

813

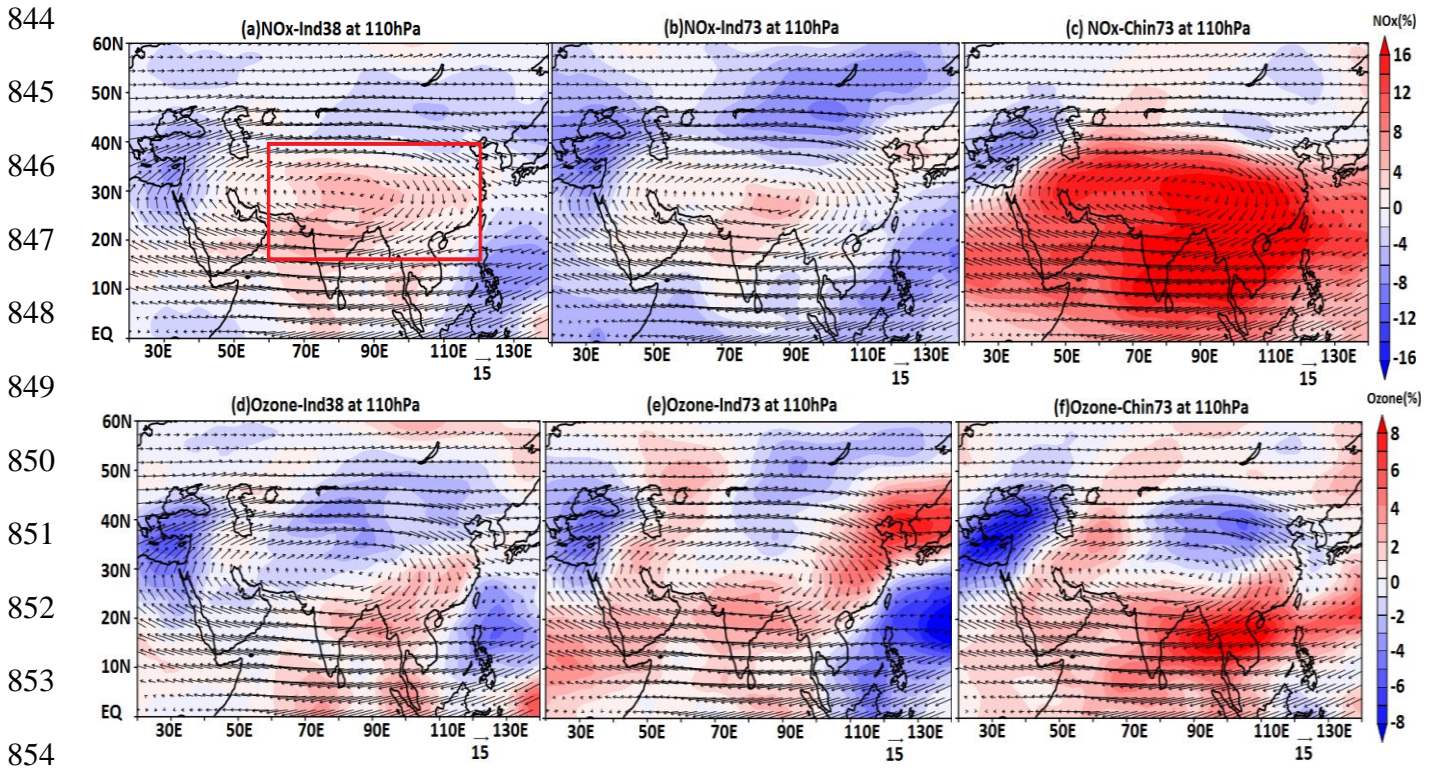
814



815 Figure 3: Longitude pressure cross-section of changes in net ozone **production (ppt/day)** due to  
816 enhanced NO<sub>x</sub> with respect to the CTRL simulation, averaged for the monsoon season (June-  
817 September) obtained from (a) Ind38 (averaged over 8°N-35°N), (b) Ind73 (averaged over 8°N-35°N),  
818 and (c) Chin73 (over 20°N-45°N) simulations. **The black line shows the tropopause while black**  
819 **contours indicate 95% confidence levels.**



836 Figure 4: Longitude pressure cross-section of percentage ozone anomalies averaged for the monsoon  
 837 season (June-September) obtained from (a) Ind38 (averaged over 8°N-35°N), (b) Ind73 (averaged over  
 838 8°N-35°N), and (c) Chin73 (averaged over 20°N-45°N) simulations. Latitude pressure cross-section of  
 839 percentage ozone anomalies averaged for the monsoon season (June-September) obtained from (d)  
 840 Ind38 (averaged over 70°E-90°E), (e) Ind73 (averaged over 70°E-90°E), and (f) Chin73 (averaged over  
 841 85°E-120°E) simulations. Black arrows indicate wind vectors. The vertical velocity field has been  
 842 scaled by 300. The **black** line represents the tropopause, and the **black dashed arrows indicate the cross**  
 843 **tropopause transport.**



855 Figure 5: Latitude-longitude cross-section of percentage NO<sub>x</sub> anomalies averaged for the monsoon  
 856 season (June-September) at 110 hPa obtained from (a) Ind38, (b) Ind73, and (c) Chin73 simulations.  
 857 Panels (d-f) show the same but for percentage ozone anomalies at 110 hPa for the (d) Ind38, (e) Ind73,  
 858 and (f) Chin73 simulations. Black arrows indicate horizontal winds at 110 hPa. **The red box in panel (a)**  
 859 **indicates the ASM anticyclone region used to compute the associated radiative forcing regional**  
 860 **average.**

861

862

863

864

865

866

867

868

869

870

871

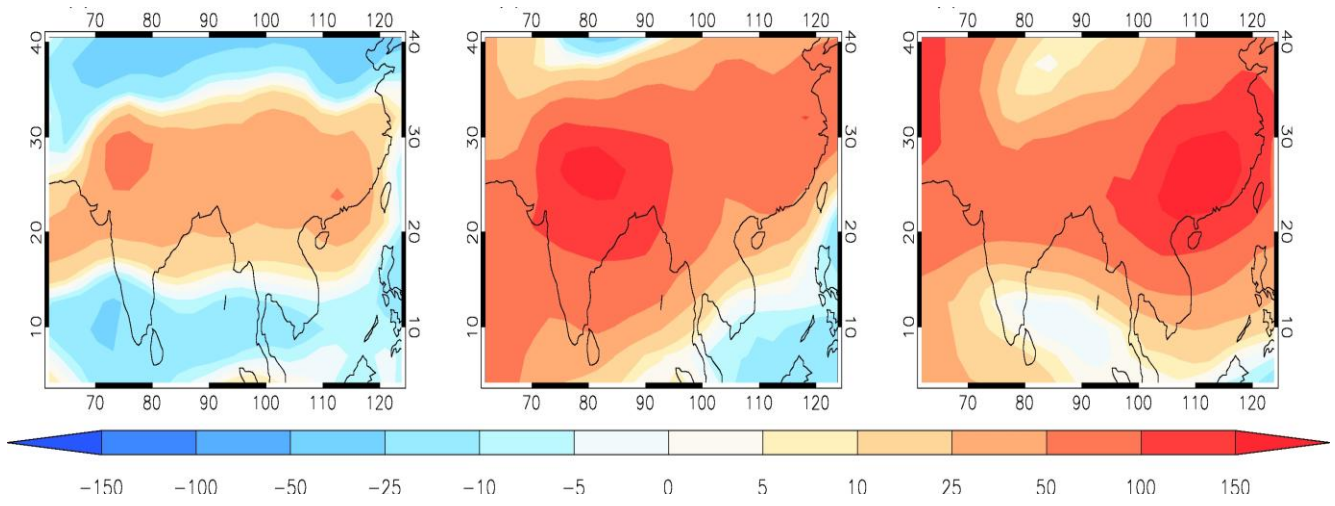


Figure 6: Latitude-longitude distribution of changes in ozone radiative forcing (in  $\text{mW m}^{-2}$ ) for the (a)

Ind38, (b) Ind73, and (c) Chin73 perturbed simulations, compared to the CTRL simulation.

872

873

874

875

876

877

878

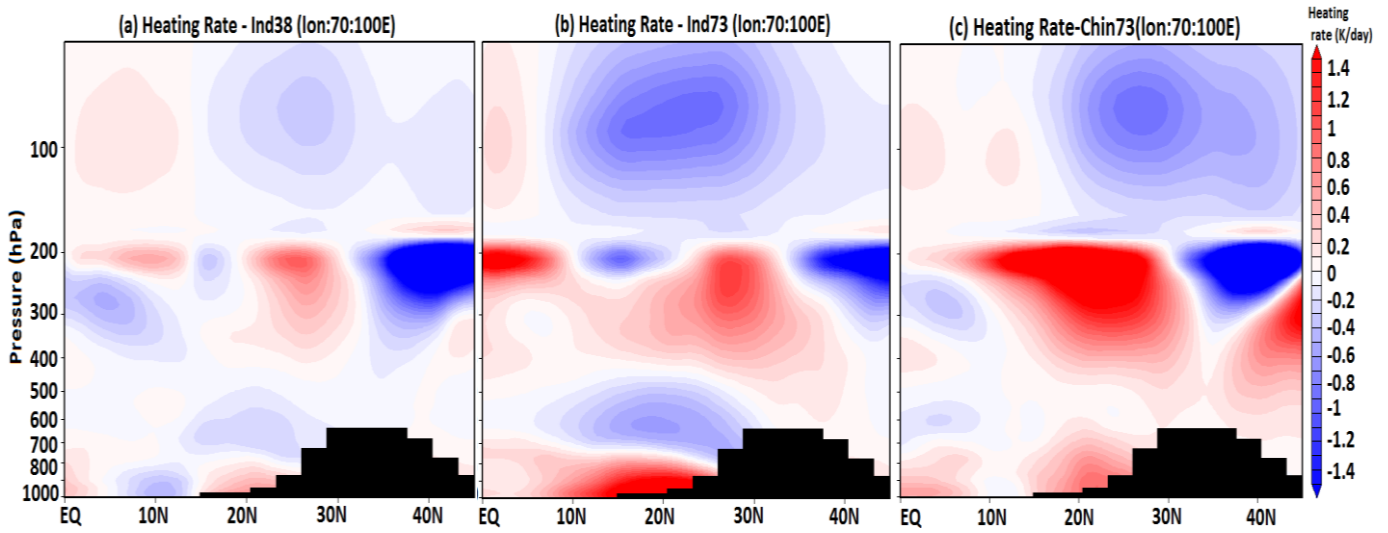
879

880

881

882

883 Figure 7: Latitude- pressure distribution of ozone heating rate changes (in K/day) for the (a) Ind38  
884 (averaged over 70°-100°E), (b) Ind73 (averaged 70°-100°E), and (c) Chin73 (averaged over 90° -100°  
885 E) perturbed simulations, compared to the CTRL simulation.





886

887

888

889

890

891

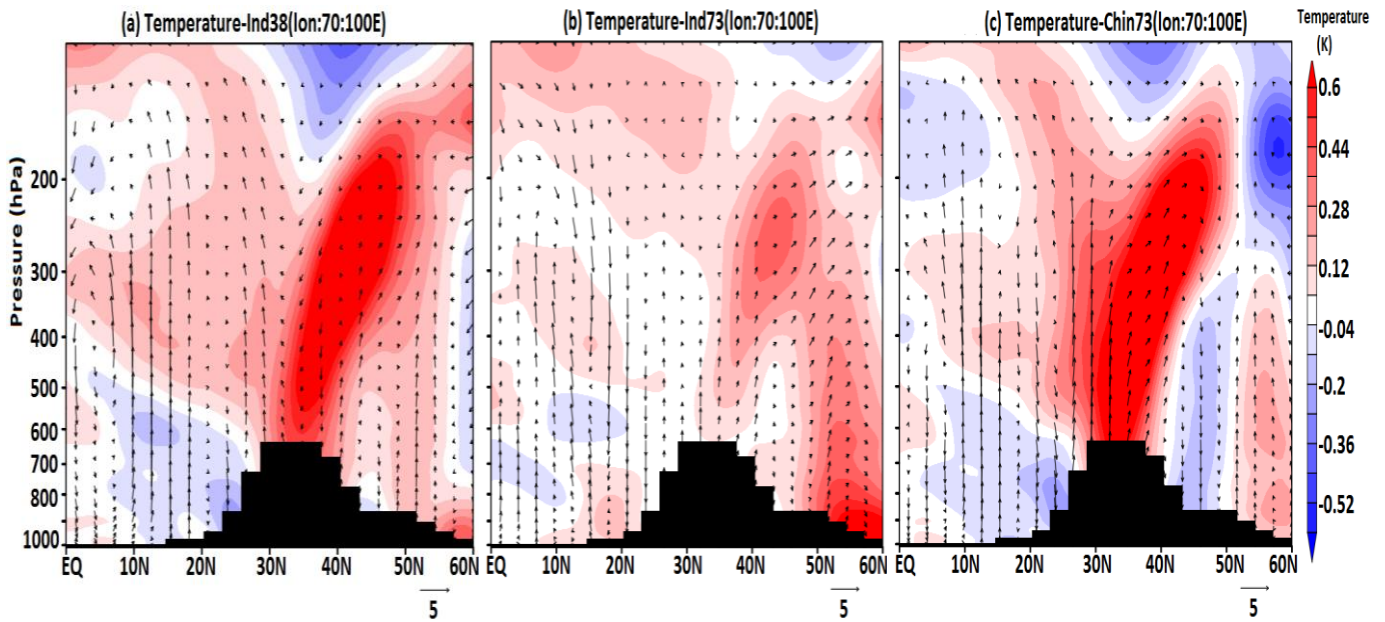
892

893

894

895

896



897

898

899

900

901

902

903

904

905

906

907

908

909

Figure 8: Latitude pressure cross-section of temperature anomalies (K) averaged for the monsoon season (June-September) and over 70°E-100°E obtained from (a) Ind38-CTRL, (b) Ind73-CTRL, and (c) Chin73-CTRL simulations. Black arrows indicate wind vectors (the vertical velocity field has been scaled by 300).

910

911

912

913

914

915

916

917

918

919

920

921

922

923

924

925

926

927

928

929

930

931

932

933

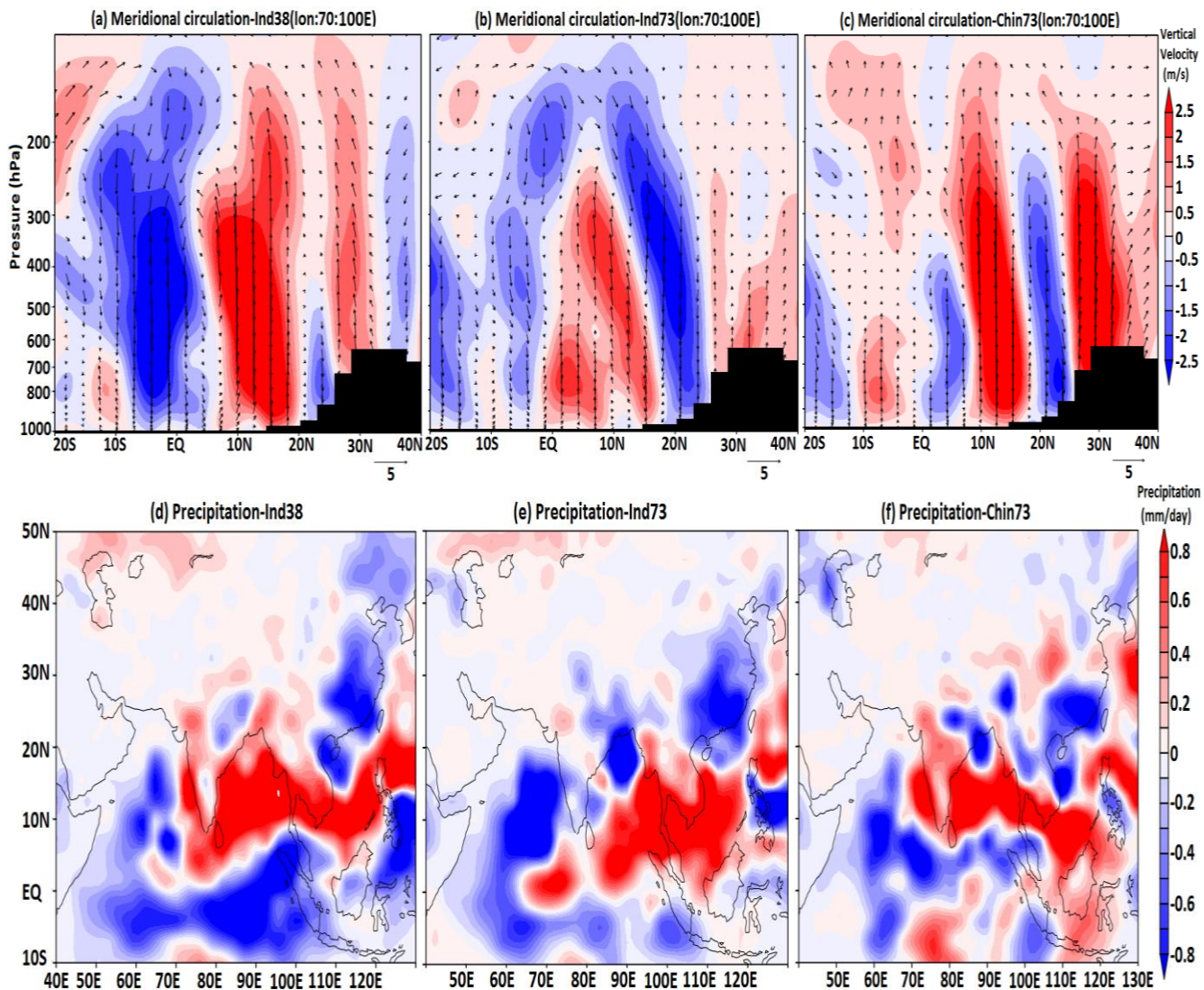


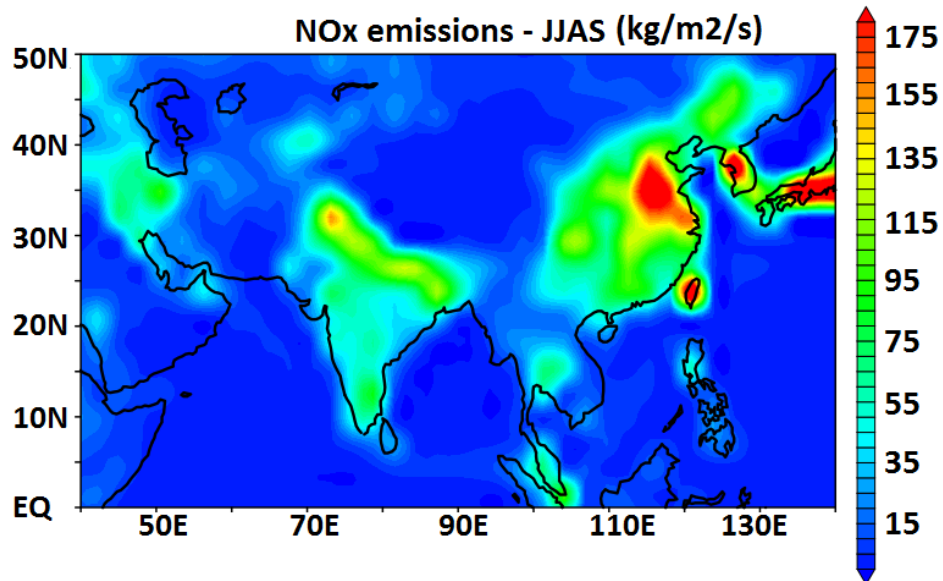
Figure 9: **Difference** in the meridional circulation due to enhanced NO<sub>x</sub> emissions averaged for the monsoon season (June-September) and over 70°E-110°E for (a) Ind38-CTRL (b) Ind73-CTRL (c) Chin73-CTRL simulations. Shaded contours indicate the anomalies in vertical velocity (m/s). **The vertical velocity field has been scaled by 300.** Precipitation anomalies (mm/day) averaged for the monsoon season (June-September) obtained from (d) India38-CTRL (e) Ind73-CTRL, **and** (f) Chin73-CTRL simulations.

934

935

## Supplementary Figures

936



937

938

939

940

941

942

943

944

945

946

947

948

949

950

951

952

953

954

Figure S1: Distribution of NO<sub>x</sub> emission mass flux ( $\text{kg m}^{-2} \text{s}^{-1}$ ) from RETRO project data set for the year 2000, averaged for the monsoon season (June-September).

955

956

957  
958  
959  
960  
961  
962  
963  
964  
965  
966  
967  
968

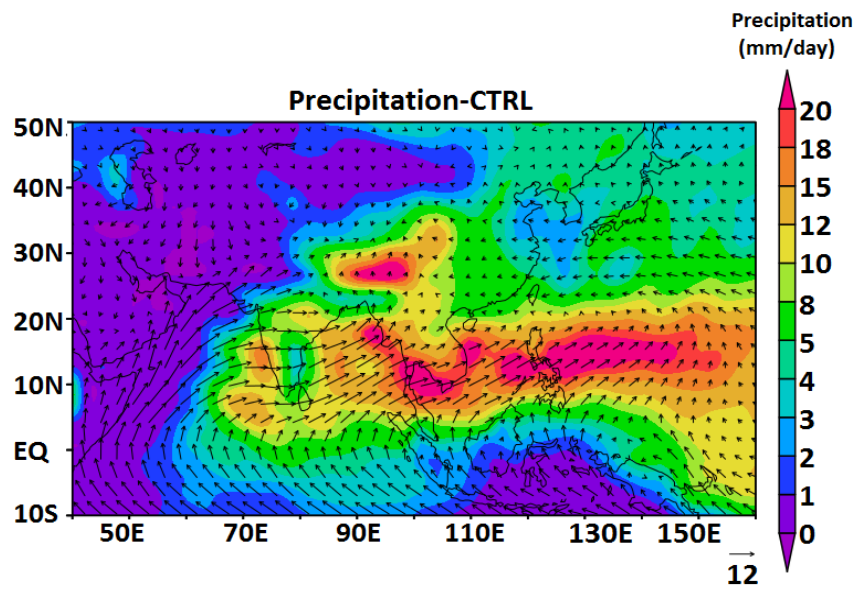


Figure S2: Distribution of seasonal (June-September) mean precipitation (mm/day) as obtained from CTRL simulation. Black arrows indicate winds (m/s).

969

970

971

972

973

974

975

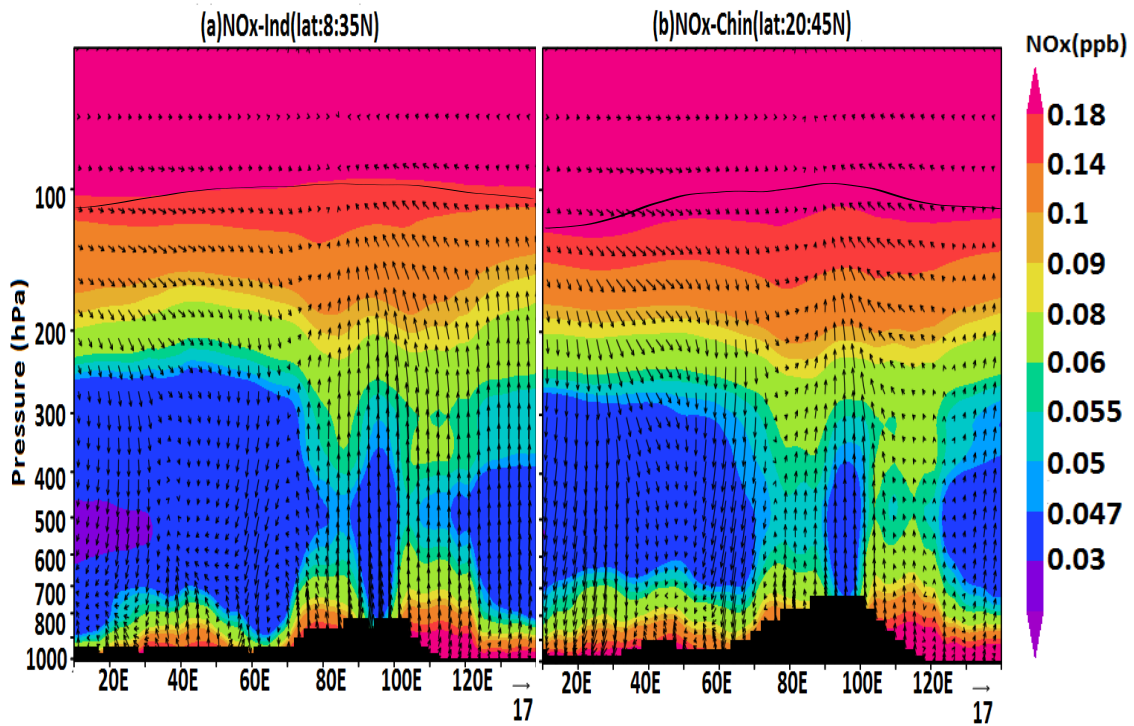
976

977

978

979

980



981

982

983

984

985

Figure S3: Vertical distribution of NO<sub>x</sub> (ppb) averaged for the monsoon season (June-September) over (a) India (8°-35°N) and (b) China (20°-45°N) as obtained from CTRL simulations. Black arrows indicate winds (m/s) (the vertical component has been scaled by 300) and the black line represents the tropopause.

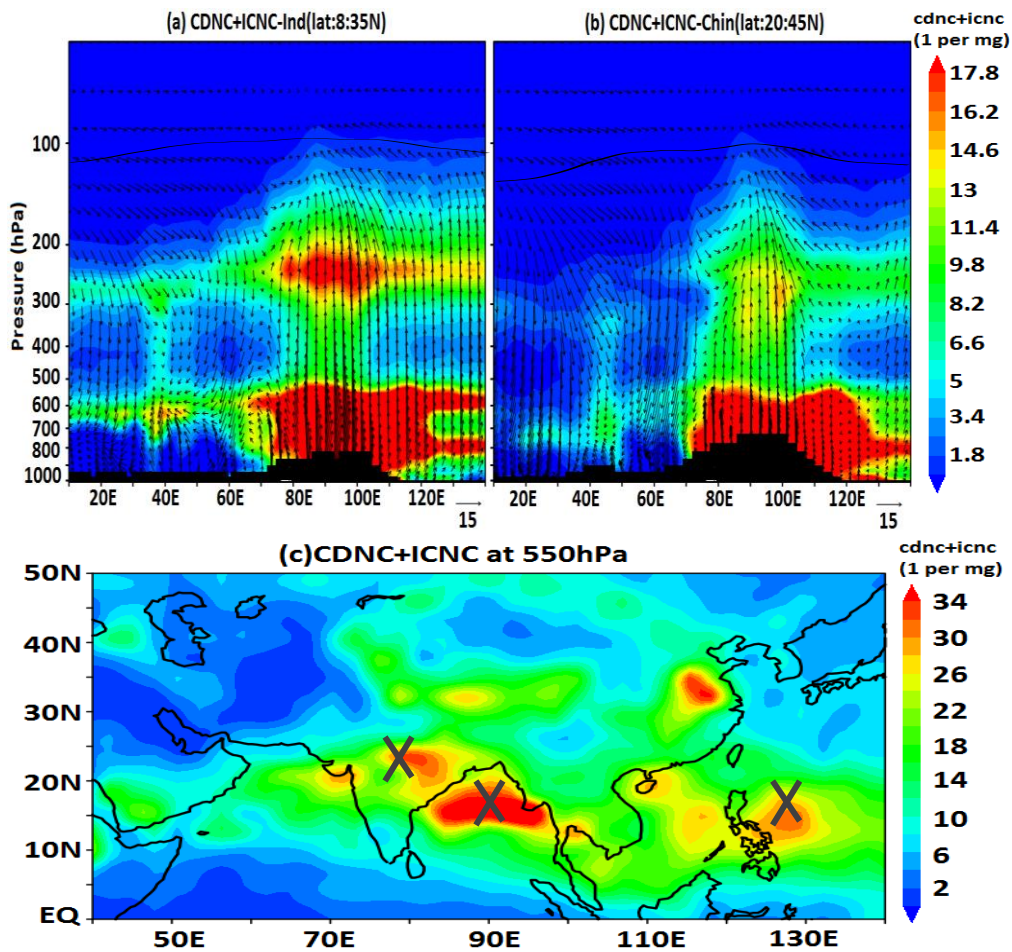
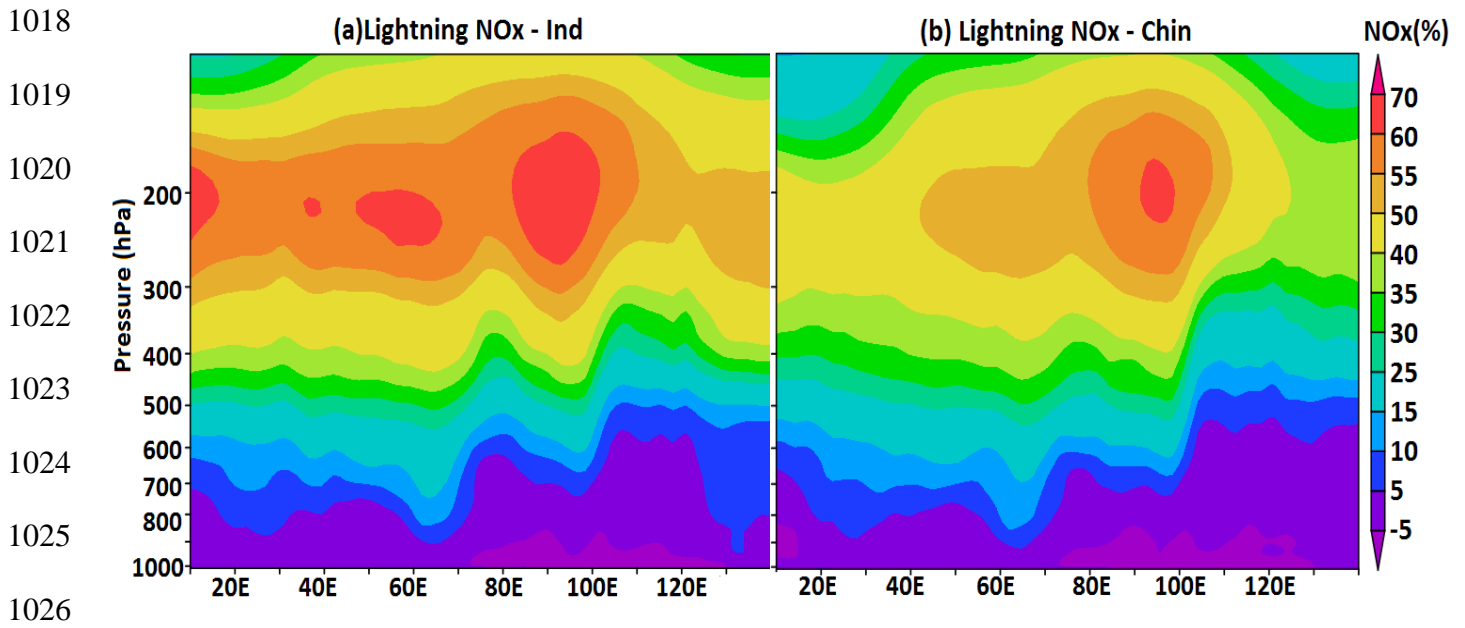


Figure S4: Distribution of combined cloud droplet (CDNC) and ice crystal (ICNC) number concentrations (in  $\text{mg}^{-1}$ ) averaged for the monsoon season (June-September) over (a) India ( $8^{\circ}$ - $35^{\circ}\text{N}$ ) and (b) China ( $20^{\circ}$ - $45^{\circ}\text{N}$ ) as simulated in the CTRL simulation. Black arrows indicate winds (m/s) (the vertical component has been scaled by 300), and the black line represents the tropopause. (c) Distribution of seasonal (June-September) mean combined CDNC+ICNC (in  $\text{mg}^{-1}$ ) at 550 hPa as simulated in the CTRL simulation. The regions of Bay of Bengal, South China Sea and southern slopes of Himalayas are indicated with a cross symbol.



1027 **Figure S5: Vertical distribution of percentage NO<sub>x</sub> anomalies produced from lightning, averaged for the**  
 1028 **monsoon season (June-September) over (a) India (8°-35°N) and (b) China (20°-45°N), simulated by**  
 1029 **comparing the CTRL-Lightning-on and the CTRL-Lightning-off experiments.**

1030

1031

1032  
1033  
1034  
1035  
1036  
1037  
1038  
1039  
1040  
1041  
1042  
1043  
1044  
1045  
1046  
1047  
1048

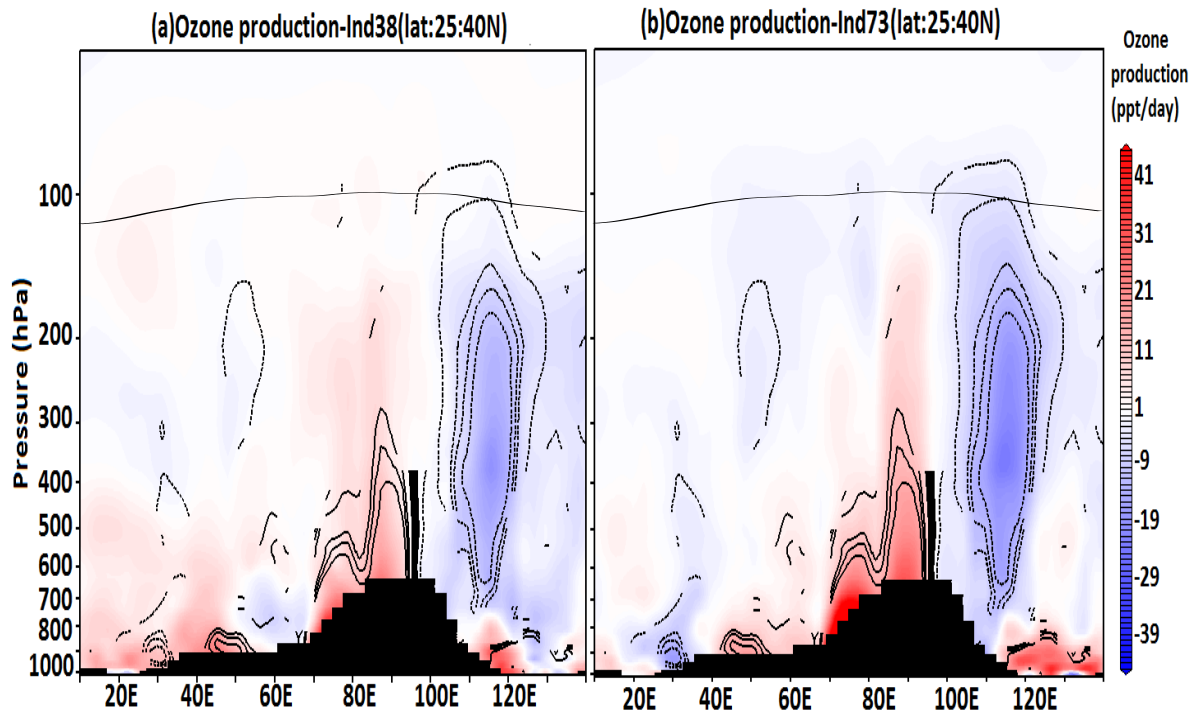


Figure S6: Longitude pressure cross-section of changes in net ozone production (ppt/day) due to enhanced NO<sub>x</sub> with respect to the CTRL simulation, averaged for the monsoon season (June-September) and over the Indo-Gangatic plain-Tibetan Plateau region (25°N-40°N) for (a) Ind38 (b) Ind73. The black line shows the tropopause while black contours indicate 95% confidence levels.